JOURNAL OF NANOSCIENCE LETTERS

Nanostructured TiO_2 architectures for environmental and energy applications

Meidan Ye[a,b], Danny Vennerberg[a], Changjian Lin[b], Zhiqun Lin[a,c,*]

[a] *Department of Materials Science and Engineering, Iowa State University, Ames, IA 50011, USA*
[b] *Department of Chemistry, College of Chemistry and Chemical Engineering, Xiamen University, Xiamen 361005, China*
[c] *School of Materials Science and Engineering, Georgia Institute of Technology, Atlanta, GA 30332, USA*

[*] *Author for correspondence: Zhiqun Lin, email: zhiqun.lin@mse.gatech.edu*
Received 19 Mar 2011; Accepted 10 May 2011; Available Online 1 Jun 2011

Abstract

Semiconductor photocatalysts have important applications in the fields of renewable energy and environmental remediation. Of these, TiO_2 stands out as one of the most investigated compounds in contemporary material science. Because of its unique physical and chemical properties, TiO_2 is extensively used in photoelectrochemical applications including photocatalysis and photovoltaics. In this Review, we focus especially on recent progress in the fabrication of TiO_2-based nanostructures. An overview of some important properties and applications of TiO_2 is given to provide context for the challenges that present research efforts aim to address. This discussion is followed by a summary of synthesis routes currently available for the preparation of nanoscale TiO_2. Finally, the various nanoarchitectures reported to date are outlined with a particular focus on their utility in photoelectrochemical applications.

Keywords: Nanostructured TiO_2; Solar cells; Photocatalysis; Hydrogen generation; Sol-gel; Hydrothermal

1. Introduction

Titanium is the ninth most abundant element in the Earth's crust. Titanium dioxide (TiO_2), which is the most common compound of titanium, is a typical n-type semiconductor. Since the inception of its commercial production in the early 20th century, TiO_2 has been widely used in pigments, paint, and toothpaste. In 1972, Fujishima and Honda observed the phenomenon of photocatalytic water splitting by a TiO_2 electrode under ultraviolet (UV) light [1]. This discovery sparked intense research of TiO_2 for applications in photovoltaics, photocatalysis, electrochromics, and sensors due to its excellent physical and chemical properties, including chemical stability, photostability and appropriate electronic band structure [2-4].

Over the past decades, an exponential increase in research effort has been devoted to nanoscience and nanotechnology. This trend is due, in part, to the amazing physical and chemical properties that emerge when a material is shrunk to nanometer scale dimensions, which creates potential barriers for electrons within the material, confining them to very small regions of space. For semiconductor nanomaterials, the movement of electron-hole pairs is primarily governed by the well-known quantum confinement effect [5]. Moreover, the confinement can be in one dimension (producing quantum films or quantum wells), in two dimensions (producing quantum wires, tubes or rods), or in three dimensions (producing quantum dots (QDs)). These three regimes are commonly referred to as 2D, 1D, or 0D, respectively, although the terms are not so precise [6-8]. Importantly, the specific surface area and surface-to-volume ratio of a material increase dramatically with decreasing size. High surface area is beneficial to many nanomaterial-based devices because it facilitates reaction or interaction between the nanomaterial and surrounding media. Thus, the performance of these devices is strongly influenced by the sizes of the material building blocks, especially at the nanometer scale [5-9].

Environmental pollution and the need for renewable energy are arguably the biggest challenges of the 21st century. With world populations booming, global energy demand has continued to rise dramatically, exhausting our fossil fuel supply at an alarming rate. A harmful and unavoidable consequence of increasing energy production based on fossil fuels is its apparent impact on the environment. For example, global warming resulting from fossil fuel greenhouse gases threatens to severely alter the climate. Additionally, the huge population and fast economic development of emerging

Table 1. Common TiO_2 crystal phases and their structural parameters (Reprinted with permission from Reference [16], Chen, S. S. et al., Chin. J. Catal. 2010, 31, 605-614. Copyright © Elsevier).

Crystal form	Crystal system	Space group	Density (g/cm^3)	Unit cell parameters			
				a/nm	b/nm	c/nm	β(°)
Anatase	Tetragonal	$I4_1/amd$	3.83	0.379	—	0.951	—
Rutile	Tetragonal	P42/mnm	4.24	0.459	—	0.296	—
Brookite	Orthorhombic	Pbca	4.17	0.918	0.545	0.515	—
TiO_2(B)	Monoclinic	C2/m	3.64	1.216	0.374	0.651	107.3

countries have introduced issues of pollution and safe waste disposal, therefore, considerable attention has been paid to these serious challenges [10,11]. In order to meet the increasing energy demand in an environmentally acceptable manner, new sustainable materials systems are necessary. Nanomaterials are emerging as promising components in alternative energy production because they offer attractive properties while requiring fewer resources to manufacture [12,13]. The enormous interest in nanoscience during the past decade has contributed to remarkable progress in environmental remediation and renewable energy technologies such as photocatalytic oxidation, solar cells, fuel cells, and biofuels [12]. The design and development of new materials and substances that are chemically modified from the molecular and atomic levels to sizes on the nanoscale has yielded structures with significantly improved properties for environmental and energy applications [14].

As the most promising photocatalyst, TiO_2 is expected to play a key role in helping ease energy shortages through effective utilization of solar energy in photovoltaic devices as well as solve many serious environmental pollution challenges via photocatalysis of pollutants. For this reason, nanostructured TiO_2 is one of the most intensely researched substances, as is evident from the more than 60,000 papers published about it over the past 50 years (with a still robustly increasing publication rate over the past decade) [4,15]. To enhance its photocatalytic ability, various morphologies of nanostructured TiO_2 including nanoparticles, nanorods, nanowires, and nanotubes have been prepared, and much progress on the synthesis of nanostructured TiO_2 with excellent catalytic properties has been made. In this Review, we focus on recent developments in the fabrication of TiO_2 nanostructures and present simplified principles of some important synthesis methods.

2. Properties

In nature, TiO_2 exists mainly in four crystal phases: anatase, rutile, brookite, and titanium dioxide (B) or TiO_2 (B). Each phase displays different physical and chemical properties supporting different functionalities. The detailed physical parameters of these four crystal phases are listed in Table 1 [16]. In general, anatase type TiO_2 has a crystalline structure that corresponds to the tetragonal system (with dipyramidal habit), and rutile type TiO_2 also has a tetragonal crystal structure (with prismatic habit). Brookite type TiO_2 has an orthorhombic crystalline structure, while TiO_2 (B) has a monoclinic structure. Since TiO_2 (B) is a relative newcomer to the TiO_2 family [17], the majority of relative investigations have primarily focused on the comparison among anatase, rutile and brookite. Rutile is the most thermodynamically stable phase for bulk TiO_2 under most conditions. However, TiO_2 generally favors the anatase structure when prepared through solution phase methods, which can be attributed to two main effects: surface energy and solution chemistry. At very small particle dimensions (i.e. the nanoscale), the transformation sequence among different TiO_2 phases is size and pH dependent because the energies of the four phases are apparently so close to one another that they can be reversed by small differences in surface energy [18,19]. All other parameters equal, anatase is most stable at diameters less than 11~14 nm, brookite is most stable for crystal sizes between 14 and 35 nm, and rutile is most stable for sizes exceeding 35 nm [20,21]. However, rutile is more stable than anatase in very acidic solutions, whereas in very alkaline solutions anatase is stabilized relative to rutile and brookite [19]. In addition to being the stable phase for bulk TiO_2, rutile is the most stable structure for nanoscale TiO_2 at high temperatures, though anatase and brookite are commonly observed in natural and synthetic nanocrystals. Under heating concomitant with

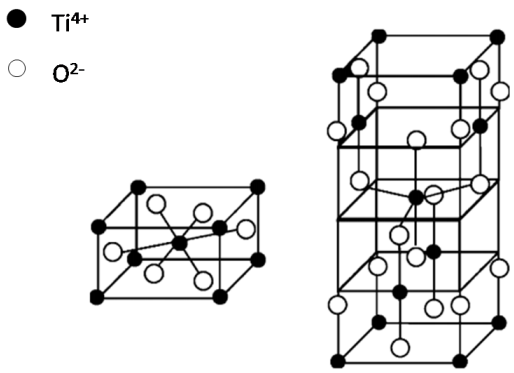

Figure 1. Schematic of crystal structure of rutile (left) and anatase TiO_2 (right). (Reprinted with permission from Reference [24], Nah, Y. C. et al., *Chemphyschem*, 2010, 11, 2698-2713. Copyright © Wiley-VCH).

coarsening, the following transformations are all favored: anatase to brookite to rutile, brookite to anatase to rutile, anatase to rutile, brookite to rutile, and TiO_2 (B) to anatase [4,16]. These transformation sequences imply very closely balanced energies as a function of particle size [22]. Even the shape transformation of the TiO_2 nanocrystals was found to be controlled by the surface chemistry, as confirmed by theoretical and experimental investigations [15,18,20,23].

Of the four phases, rutile and anatase are the most practically important crystal structures, and Figure 1 shows their unit cell structures. These two structures can be described in terms of chains of TiO_6 octahedra, where each Ti^{4+} ion is surrounded by six O^{2-} ions. The two crystal structures are different in the distortion of each octahedron as well as the assembly pattern of the octahedra chains. That is, within rutile, the octahedron exhibits a slight orthorhombic distortion, whereas in anatase, the octahedron is significantly distorted so that its symmetry is lower than that of orthorhombic. Moreover, the Ti-Ti distances of anatase are larger and the Ti-O distances are shorter than those in rutile. In assembling the rutile structure, each octahedron is in contact with ten neighboring octahedrons (two sharing edge oxygen pairs and eight sharing corner oxygen atoms). In the anatase structure, each octahedron couples to eight neighbors (four sharing an edge and four sharing a corner) [4,15,24,25]. Accordingly, these distinctions in lattice structures produce differences in electronic properties between the two phases of TiO_2. Generally, anatase appears to be the more photoactive than rutile. This is probably because of the differences in the extent and nature of the surface hydroxyl groups present in the low

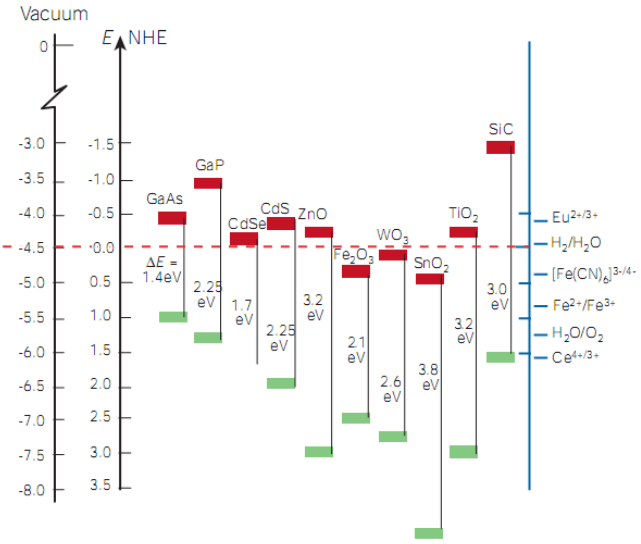

Figure 2. Band gap energies and band positions of several semiconductors in contact with aqueous electrolyte at pH 1. (Reprinted with permission from Reference [14], Gratzel, M. Nature 2001, 414, 338-344. Copyright © Nature Publishing Group).

temperature anatase structure. Furthermore, the photoactivity enhancement can be related to the Fermi level of anatase (a band gap of 3.2 eV) which is about 0.2 eV higher than that of rutile (a band gap of 3.02 eV) [2,26]. However, rutile TiO_2 still has some advantages over anatase such as higher chemical stability, higher refractive index, and cheaper production cost, while also performing comparably to anatase in photocatalysis application [27]. Additionally, monoclinic TiO_2 (B) has a relatively open structure with large voids and continuous channels, which endows it with fast transport paths for lithium intercalation as well as excellent photoelectrical properties [15,28]. Comparatively, orthorhombic brookite TiO_2 is theoretically predicted to be a promising dielectric with a static dielectric constant much higher than anatase and rutile. This is most likely because brookite is a metastable phase with a very complicated and low symmetry structure and as a result of the rapid transformation that accompanies secondary phases such as anatase or rutile [29]. More importantly, considerable results have demonstrated that mixtures of different phases, such as anatase/rutile [30], anatase/brookite [21], and brookite/rutile [21] (anatase/rutile in particular), possess synergistically enhanced charge-carrier transfer, which improves their performance in photocatalytic applications [3].

The electronic properties of TiO_2 have been investigated by using a variety of theoretical studies and experimental techniques [2,15,24,31-36]. In brief, TiO_2 is an n-type semiconductor comprised of a conduction band with an edge of low energy formed by the vacant Ti^{4+} d bands, and a valence band with an upper edge composed of O^{2-} filled pπ bands [24]. The band-gap energy of indirect electron transition is 3.02 and 3.2 eV for rutile and anatase, respectively. Apart from these definite band gap values, the relative position of energy levels compared to redox potentials of some species in media are of great importance for numerous functional applications of TiO_2, which will be discussed in the following section.

3. Applications

Since the discovery of hydrogen evolution through the photoelectrochemical splitting of water based on n-type TiO_2 electrodes by Fujishima and Honda in 1972 [1]. semiconductor photocatalysts have attracted great attention from both academic and industrial communities. In particular, TiO_2 nanomaterials have found wide application in the fields of dye-sensitized solar cells, hydrogen production, the degradation of organic pollutants, sensors [37], and photoinduced hydrophilicity [38], to name a few. Herein, the application of TiO_2 nanomaterials in solar cells, hydrogen generation, and photocatalytic degradation of organic pollutants are discussed in detail to illustrate some promising alternatives for renewable energy exploitation and environment protection.

3.1. Dye-sensitized solar cells

Solar energy is clean, silent, and endlessly abundant, making it one of the most promising future energy resources. The direct conversion of sunlight into electrical power by solar cells is of particular interest because of its many advantages over currently used electrical power generation methods. For instance, solar-based electricity is obtained without the exhaust of green-house gases or nuclear waste by products [12,13]. To date, silicon remains the dominant material for solar cell systems [7]. However, the inherent deficiencies of silicon solar cells, such as the complicated and energy intensive fabrication process and inevitable use of toxic chemicals, along with the heavy cell weight and the high manufacturing costs, have aroused a strong desire to develop cost-efficient, versatile, and easily manufacturable alternatives to the silicon status quo [35,39]. A dye-sensitized solar cell (DSSC), also known as the Gratzel cell, was first announced in 1991 with a conversion yield of 7.1% [40]. This promising electrochemical device relies on an operating principle similar to the photo-synthesis reaction of green plants. The DSSC is attractive for its simple manufacturability, low cost, and use of abundant and non-toxic materials [39,41]. In addition, DSSCs performs better under illumination from low light intensities and diffuse light conditions than traditional silicon solar cells, which makes them especially suitable for low-power indoor applications such as laptop computers and mobile phones. DSSCs can also be fabricated on flexible substrates such as plastic foils and metal sheets, making them suitable for large scale, roll-to-roll type industrial manufacturing processes [39]. In short, DSSCs offer the possibility of designing photovoltaics with tunable shape, color, and transparency as well as feasible integration into large-scale commercial products [35,42].

Typically, a DSSC consists of five components: a conductive mechanical support, a semiconductor film, a sensitizer, an electrolyte and a counter electrode. Hence, the total efficiency of DSSCs depends on the optimization and compatibility of each of these constituents [43]. In DSSCs, electricity is created at the photoanode, which is formed of nanostructured TiO_2 materials covered with a monolayer of

visible light absorbing dye [44]. Photon absorption generates excitons in the dye via a metal-to-ligand type transition, and the excited electrons are efficiently injected into the TiO_2 conduction band, which is significantly lower than the excited state of the dye molecule. The electrons diffuse through the TiO_2 nanomaterial into the current collector (e.g. transparent conductive glasses), from which they can be transferred into an external load [6,41,42,45]. Efficient collection of solar power begins with sensitizing dyes, which should possess several properties including stability, wide spectral absorbance range, and a molecular structure suitable for chemical bonding on TiO_2 materials. The most commonly used dyes are organometallic ruthenium polypyridyl complexes (e.g. N719 dye[ruthenium(2,2'-bipyridyl-4,4'-dicarboxylate)$_2$(NCS)$_2$]), which satisfy almost all of the above requirements [42,46-48]. However, because ruthenium is a rare metal, alternative dyes containing no metal or only inexpensive metals have been developed for DSSCs [49]. In addition to organometallic dyes, quantum dots have also been explored as a substitute for dyes because of the visible light response ability of some kinds of quantum dots (e.g. CdS, CdTe, and CdSe), nevertheless, the conversion efficiency of these quantum dot solar cells (QDSSCs) is still much lower than DSSCs, mostly due to their instability when exposed to visible light [50-52].

The photoanode in a DSSC is coupled with the counter electrode (CE) through a layer of redox-electrolyte separating the two electrodes. The redox-electrolyte plays the important role of transporting positive holes generated during dye excitation to the counter electrode, which is realized by alternating the oxidation states of dye molecules on the photoanode. The reduced species of the couple (e.g. iodide or I^-) contained in the redox electrolyte donates electrons to the oxidized dye to reduce it back to the ground state where it can absorb photons again. The redox species renews the oxidized state by itself (e.g. I^- to I_3^-) and diffuses to the counter electrode, where electrons returning from the external load reduce the redox species back to its original state (e.g. I_3^- to I^-). The reduced redox species then diffuses back to the photoanode to start a new reaction circle [6,41,42]. To date, the I^-/I_3^- redox couple, in conjunction with ruthenium polypyridyl dyes, has displayed the highest power conversion efficiencies in DSSCs, and thus, this redox couple is utilized in practically all liquid or quasi-solid DSSC electrolytes [53]. I^- ions are typically introduced from an alkali metal salt such as LiI or an imidazolium derivative called ionic liquid electrolyte, and I_3^- emerges when I^- react with I_2 in the electrolyte. Besides the I^-/I_3^- redox couple, the electrolyte commonly contains other species such as 4-tert-butylpyridine (TBP), which attach to sites on the TiO_2 surface not covered with dye in order to suppress dark current in the cell. In addition, several low-viscosity solvents are present in the electrolyte to ensure that all constituents remain dissolved in solution, for example, various nitriles (aceto-, methoxypropio-, valero- or butyronitrile) or mixtures of carbonates (ethylene/ propylenecarbonate) are found in many electrolytes. A typical electrolyte consists of methoxyproprionitrile (MPN) with 0.1~0.5 M LiI, 0.1~0.5 M TBP, and 0.1 M I_2 [53,54]. However, in the case of liquid electrolytes, cell degradation is caused by solvent evaporation and leakage over time. Accordingly, polymers can be added to the ionic liquid to form the electrolyte into quasi-solid gel (resembling solid state solar cells) to minimize leakage [41,43,55,56].

As mentioned above, the counter electrode returns charge from the external circuit back to the cycling circuit in the cell. Thus, an active catalyst layer coated on the counter electrode surface is necessary to achieve sufficient charge transfer. Platinum is the most commonly used counter electrode material because of its high catalytic activity for the triiodide reduction reaction, chemical inertness, and mechanical stability [6,41,42]. However, the shortage and high price of platinum metal has inspired the pursuit of other catalysts such as activated carbons, carbon nanomaterials and p-type conducting polymers [55,57,58].

Roughly, the overall operating cycle in DSSCs can be described in Figure 3 and in the following reactions [6,43]. Of note are deleterious recombination processes within a DSSC involving the recombination of photoexcited electrons with electron acceptors, such as oxidized ions and electron scavengers located in the electrolyte or oxidized dye molecules at the dye-electrolyte interface [59]. Several excellent reviews provide detailed discussions of the kinetic and energetic behavior of photoexcited electrons in DSSCs [41,44,54,59,60].

$$S\,(TiO_2) + h\nu \rightarrow S^*$$
light absorption by the dye molecules (1)

$$S^* \rightarrow S^+ + e^-\,(TiO_2)$$ electron injection (2)

$$e^-\,(TiO_2) \rightarrow e^-\,(\text{current collector})$$
electron transport (3)

$$2S^+ + 3I(TiO_2) \rightarrow 2S + I_3\,(TiO_2)$$
dye regeneration (4)

$$I_3^-\,(TiO_2) \rightarrow I_3^-\,(CE)$$ tri-iodide diffusion (5)

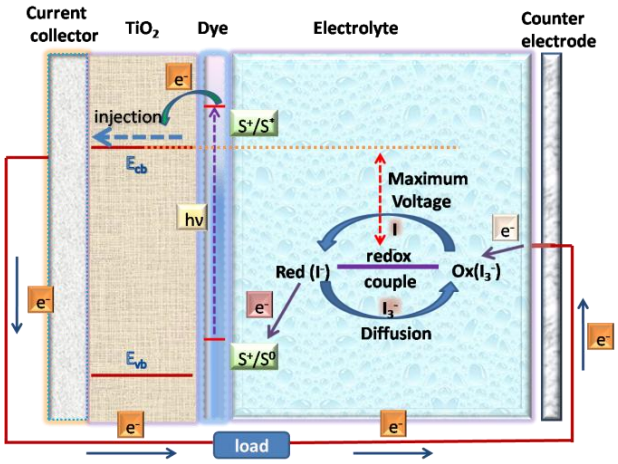

Figure 3. The operating principle of DSSCs based on TiO_2 nanomaterials.

$$I_3^-(CE) + 2e^-(CE) \rightarrow 3I^-(CE) \quad \text{iodide regeneration} \quad (6)$$

$$3I\,(CE) \rightarrow 3I\,(TiO_2) \quad \text{iodide diffusion} \quad (7)$$

DSSC performance can be effectively characterized using the following parameters: maximum short-circuit current (J_{sc}), open-circuit photovoltage (V_{oc}), fill factor (FF), and overall solar-to-electrical energy conversion efficiency (η) [54]. For a solar cell, η can be determined using equation (8), where P_{in} is the intensity of the incident light. The FF can assume values between 0 and 1 and is defined by the ratio of the maximum power (P_{max}) generated by the solar cell per unit area to the V_{oc} and J_{sc} according to equation (9). P_{max} is obtained from the product of the photocurrent and photovoltage at the voltage where the power output of the cell is maximal [48]. Another fundamental evaluation of solar cell performance is "external quantum efficiency", which is normally called the incident photon to current conversion efficiency (IPCE). IPCE values provide useful information about the monochromatic quantum efficiencies of a solar cell since they are defined by the photocurrent density generated in an external circuit under monochromatic illumination of the cell divided by the photon flux that hits the cell. IPCEs can be calculated from equation (10), where e is the elementary charge [60].

$$\eta = \frac{J_{sc}V_{oc}FF}{P_{in}} \quad (8)$$

$$FF = \frac{P_{max}}{J_{sc}V_{oc}} \quad (9)$$

$$IPCE = \frac{J_{sc}(\lambda)}{e\phi(\lambda)} = 1240\frac{J_{sc}(\lambda)[Acm^{-2}]}{\lambda[nm]P_{in}(\lambda)[Wcm^{-2}]} \quad (10)$$

As the core of DSSCs, TiO_2 nanomaterials not only need to transport the photoexcited electrons into current collectors as quickly as possible, but also need to serve as effective anchors for sensitized dyes to adsorb to. To date, an approximately 10-μm thick film with a 3D network composed of interconnected spherical TiO_2 nanoparticles (NPs), has obtained an overall power conversion efficiency of over 11% [61]. However, in this disordered network numerous grain boundaries are believed to restrict the excited electron transport. In this regard, considerable research is devoted to the fabrication of various nanostructured TiO_2 materials, such nanospheres, nanotubes, nanorods, nanowires and combined structures in order to alleviate this blockage of current flow.

3.2. Photocatalytic hydrogen generation

In the face of fossil-fuel shortages and worsening environmental pollution, hydrogen-based energy systems have attracted extensive attention. Hydrogen is a clean energy because chemical energy stored in the H-H bond is easily released when the molecule reacts with oxygen to yield water as a byproduct. In order to realize a hydrogen economy, future energy devices capable of generating hydrogen sustainably will be necessary. In addition to holding promise as an energy source, hydrogen is also a versatile energy carrier that is currently produced from a variety of primary sources such as natural gas, heavy oil, methanol, biomass, wastes, coal, solar, wind and nuclear power. Among these sources, hydrogen production using solar irradiation attracts the greatest attention because of its potential to utilize solar energy to split water in the form of heat, light, or electricity. The direct use of sulnight provides the most efficient route of hydrogen production because it avoids the inefficiencies ascribed to thermal transformation or electrolysis following the conversion of solar

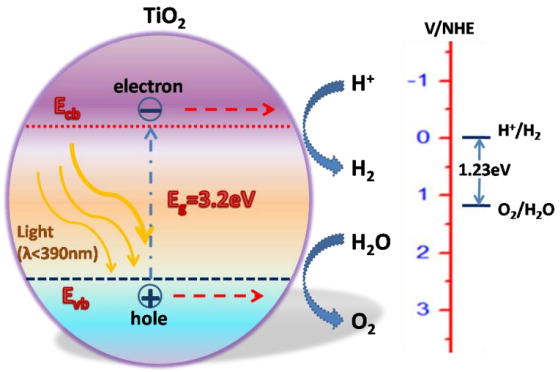

Figure 4. Overview principle of TiO_2-based photocatalytic water splitting for hydrogen generation.

energy to electricity [12,13,62]. Water decomposition using sunlight in the presence of semiconductor photocatalysts has attracted intense research interest since the pioneering work on a photo-electrochemical cell demonstrated by Honda and Fujishima in 1972 [1].

Thermodynamically, the overall water-splitting reaction is an uphill reaction with a significantly positive change in Gibbs free energy (ΔG^0=+237.2 kJ/mol, 1.23 eV per electron). The absorbed photon energy needs to overcome this large Gibbs free energy for water splitting [62]. Since the electrochemical decomposition of water to hydrogen and oxygen is a two-electron stepwise process, it is feasible to use photocatalytic surface reactions which rely on solar energy to generate electrons and holes that can respectively reduce and oxidize the water molecules adsorbed on photocatalysts. However, the applied semiconductor photocatalyst should possess band gap energy (Eg) greater than 1.23 eV to overcome the Gibbs free energy for hydrogen generation. In addition, the band position of the photocatalyst is also important. That is, for easy electron-hole pair transfer, the semiconductor conduction band should be located at a potential more negative than the reduction potential of water, while its valence band should be located at more positive position than the oxidation potential of water [1,62-66].

It has been published that some metal oxides, (for instance, TiO_2, $SrTiO_2$, ZrO_2, $BaTi_4O_9$, and CeO_2) possess reasonable activities for water splitting into H_2 and O_2 in the stoichiometric ratio under ultraviolet (UV) or visible light irradiation [62]. TiO_2 has been widely used in photocatalysis, owing to its favorable band-gap energy (3.2 eV in anatase) and high stability in aqueous solution under UV irradiation. The photocatalytic process of TiO_2 is initiated by the absorption of a photon with energy matching or greater than the forbidden band gap energy of the semiconductor. Subsequently, electron-hole pairs are generated following light irradiation. Photoexcited electrons migrate to the conduction band where they reduce H^+ to H_2 (see reactions 11 and 12, Figure 4), and holes on the surface of the semiconductor decompose H_2O to O_2 (see reaction 13 and 14, Figure 4) [4,62,64,66,67].

$$TiO_2 \xrightarrow{h\upsilon > E_g} TiO_2(e^-_{cb} + h^+_{vb}) \quad (11)$$

$$2e^-_{cb} + 2H^+ \rightarrow H^{\cdot} + H^{\cdot} \rightarrow H_2 \quad (12)$$

$$h^+_{vb} + H_2O \rightarrow H_2O^+ \rightarrow OH^{\cdot} + H^+ \quad (13)$$

$$OH^{\cdot} + OH^{\cdot} \rightarrow H_2O + \frac{1}{2}O_2 \quad (14)$$

However, in order to be excited by visible light irradiation, the band gap energy of the semiconductor should be less than 3.0 eV. Consequently, although the large band gap of TiO_2 (3.2eV for anatase) is crucial for many applications, it hampers the efficient utilization of visible light (only about 7% of solar energy in the spectral range has a wavelength less than 400 nm). Therefore, remarkable efforts have focused on modifying the electronic properties of TiO_2 through shortening the optical band gap, doping the material, or suitable modification of the TiO_2 surface (sensitization or junction formation) to create a valuable visible-light response [3,4,24,62,64]. In a simple aqueous solution, pure TiO_2 cannot split water into H_2 and O_2 because of the fast, undesired electron-hole recombination reaction, which is thermodynamically favored. To counter this deleterious reaction, so-called sacrificial reagents are added to the water. Their main function is to separate the photoexcited electrons and holes that are available for reversible reaction by playing the role of electron donors or electron-acceptor scavengers. For photocatalytic hydrogen generation, compounds such as methanol, ethanol, EDTA, Na_2S, $NaCO_3$,

Na_2SO_4, or ions such as I^-, IO_3^-, CN^-, and Fe^{3+} can be used as sacrificial reagents [67].

The efficiency of photocatalytic hydrogen generation from water splitting can be measured directly from the amount of generated hydrogen gas or indirectly from the electrons transferred from semiconductor to water within a certain time period under light irradiation. Commonly, the rate of gas (O_2 and H_2) evolution with units such as $\mu mol \cdot h^{-1}$ and $\mu mol \cdot h^{-1} \cdot g^{-1}$ is used to make measurable comparisons between different photocatalysts under similar experimental conditions. Another measure of photocatalytic activity, the (apparent) quantum yield, is an extension of the overall quantum yield in a homogeneous photochemical system, and these parameters can be calculated by equation 15 and 16, respectively. In addition to quantum yield, the solar energy conversion efficiency that is usually used for evaluation of solar cells is also sometimes applied and estimated by equation 17 [66].

$$\text{Overall quantum yield}(\%) = \frac{\text{Number of reacted electrons}}{\text{Number of absorbed photons}} \times 100\% \quad (15)$$

$$\text{(Apparent) Quantum yield}(QY, \%) = \frac{\text{Number of reacted electrons}}{\text{Number of incident photons}} \times 100\% = \frac{2 \times \text{Number of evolved } H_2 \text{ molecules}}{\text{Number of incident photons}} \times 100\%(\text{for } H_2 \text{ evolution}) = \frac{4 \times \text{Number of evolved } O_2 \text{ molecules}}{\text{Number of incident photons}} \times 100\%(\text{for } O_2 \text{ evolution}) \quad (16)$$

$$\text{Solar energy conversion}(\%) = \frac{\text{Output energy of hydrogen evolved}}{\text{Energy of incident soalr light}} \times 100\% \quad (17)$$

Significantly, TiO_2 was the first discovered photocatalyst for water splitting under UV irradiation, where the corresponding quantum efficiency was approximately 10% in the case of Fe^{3+} doping [1]. Furthermore, colloidal TiO_2 combined with Pt and RuO_2 particles generated H_2 and O_2 in stoichiometric proportions from water with a high quantum yield of 30±10% under UV irradiation [66]. Other published results about hydrogen generation from water splitting via solar irradiation based on TiO_2 nanomaterials will be shown in later sections.

3.3. Photocatalytic degradation of organic pollutants

As industrialization and population growth have spiked in recent years, the environmental contamination caused by wastewater pollutants has become a worldwide problem. Wastewaters from various industries pose a serious environmental threat because they contain organic pollutants that are toxic to microorganisms, aquatic life, and human beings [17,68]. In the past decades, conventional biological and physical treatment methods, such as adsorption, ultrafiltration, and coagulation have served as popular techniques to remove the organic pollutants from various wastewaters [17]. However, novel techniques are actively being pursued for the decontamination of many artificial or anthropogenic organic pollutants, especially those with high toxicity but very low concentration. These techniques should be able to chemically transform the organic pollutants into non-hazardous compounds efficiently and rapidly. Semiconductor nanomaterials hold promise for inexpensive and environmentally friendly decontamination systems, in which the correlated chemical reagents, energy source and catalysts could be abundant, cheap, and nontoxic, while producing no secondary pollution byproducts [68,69].

Recently, considerable studies have been devoted to the utilization of photocatalysis in the degradation of organic pollutants from wastewaters, particularly due to its ability to completely mineralize the toxic organic chemicals into non-toxic inorganic minerals [5,17,63,68,69]. Photocatalysis is a photoinduced reaction that can be improved by using a catalyst. Semiconductors (such as TiO_2, ZnO, Fe_2O_3, CdS, and ZnS) can serve as sensitizers for light-induced redox-reactions because of their unique electronic structure, which is characterized by a filled valence band, and an empty conduction band [5]. Under irradiation, the valence band electrons are excited to the conduction band leaving a hole behind. The resulting electron–hole pairs can recombine or react separately with other molecules. The holes may migrate to the surface and react either with electron donors in the solution or with hydroxide ions to produce powerful oxidizing species like hydroxyl or superoxide radicals. Meanwhile, the conduction band electrons can reduce an electron acceptor. Consequently, semiconductor materials can act as either an electron donor or an electron acceptor for molecules in the surrounding medium, depending on the charge transfer to the adsorbed species [63,70]. Compared to other semiconductors, TiO_2 is the most widely used semiconductor catalyst in photoinduced processes because it is chemically and biologically inert, photostable, relatively easy to manufacture and utilize, able to efficiently catalyze reactions, inexpensive, and nontoxic, though it has the disadvantage of activation only by ultraviolet (UV) light and not visible irradiation [5,15 68,71].

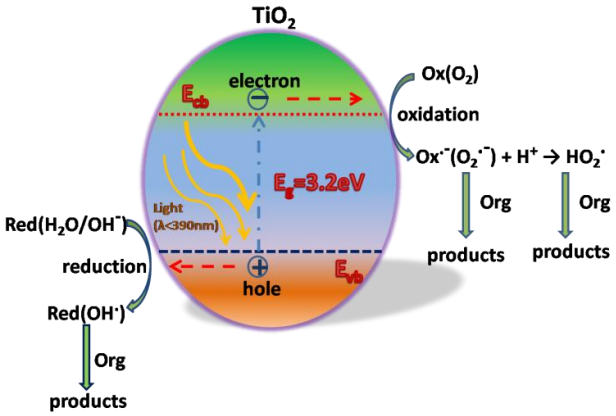

Figure 5. Simplified principle of TiO_2-based photocatalysis of organic pollutants.

In TiO_2, the photocatalytic reactions are principally activated by absorption of a photon with sufficient energy (equal to or higher than the band gap energy (Eg) of TiO_2) to produce an electron-hole pair. The photoexcited electrons can react with O_2, reducing it to superoxide radical anion, $O_2^{-\bullet}$, or reduce the organic chemicals, which act as the electron acceptors adsorbed on the TiO_2 surface or dissolved in water. Meanwhile, the photogenerated holes can oxidize organic molecules to form oxidized products or react with OH^- or H_2O to form $OH^\bullet$ radicals. The resulting $^\bullet OH$ radical, a very strong oxidizing agent (standard redox potential +2.8V), can oxidize most organic chemicals to mineralized products [72,73]. Accordingly, the relevant reactions on the TiO_2 surface resulting in the degradation of organic pollutants can be expressed in the following reactions as well as in Figure 5 [17,68].

$$TiO_2 + h\upsilon(UV) \rightarrow TiO_2(e^-_{CB} + h^+_{VB}) \quad (18)$$

$$TiO_2(h^+_{VB}) + H_2O \rightarrow TiO_2 + H^+ + OH^\cdot \quad (19)$$

$$TiO_2(h^+_{VB}) + OH^- \rightarrow TiO_2 + OH^\cdot \quad (20)$$

$$TiO_2(e^-_{CB}) + O_2 \rightarrow TiO_2 + O_2^{-\cdot} \quad (21)$$

$$O_2^{-\cdot} + H^+ \rightarrow HO_2^\cdot \quad (22)$$

$$Org + OH^\cdot \rightarrow \text{degradation products} \quad (23)$$

$$Org + h^+_{VB} \rightarrow \text{oxidation products} \quad (24)$$

$$Org + e^-_{CB} \rightarrow \text{reduction products} \quad (25)$$

However, for organic chemical degradation, TiO_2 materials still suffer the limitation of activation solely by UV light ($\lambda <$ 390 nm). Therefore, several remediation strategies have been employed, for instance, the bulk-doping approach is frequently used to develop TiO_2-based visible-light-response photocatalytic systems [3,68].

4. Synthesis methods

Recently, TiO_2 nanomaterials, including nanoparticles, nanorods, nanowires, and nanotubes have been widely investigated, and various synthesis methods, including, sol-gel [74,75], hydrothermal/solvothermal [76], physical/chemical vapor deposition [31], electrochemical anodization, and direct chemical oxidation [15,77], have been successfully applied in fabricating them. In this section, some popular methods are discussed with a specific focus on the properties of TiO_2 nanostructures attained from each technique.

4.1. Sol-Gel

TiO_2 nanomaterials have been frequently synthesized via the sol-gel method, a widely used method in making various ceramic materials. In a typical sol-gel process, a colloidal suspension or sol is formed from the hydrolysis and polymerization reactions of the precursors, which are usually inorganic metal salts or metal organic compounds such as metal alkoxides. Subsequent complete polymerization and loss of solvent induces a phase conversion from the liquid sol into a solid gel phase. Furthermore, this technique allows for the production of thin films on a variety of substrates by spin-coating or dip-coating. Hence, nanomaterials with novel properties can be obtained via the sol-gel process under optimized conditions. TiO_2 synthesis using the sol-gel method occurs from the hydrolysis of a titanium precursor, and this process is normally performed via an acid-catalyzed hydrolysis step of titanium (IV) alkoxide or halide precursor followed by condensation. Properties of the resulting nanomaterials, such as the degree of crystallinity, morphology, structure size, surface area, and degree of agglomeration, depend on the reaction conditions, including the temperature,

evaporation rate, drying conditions, and post-treatment. The rates of hydrolysis and condensation are largely affected by the type of precursors, the pH, and the mixture of solvents [4,15,74]. Among various methods, the sol–gel method is one of the most widely used for TiO_2 nanostructure preparation, due to its advantages of relatively low cost, flexibility of substrate (several sizes and shapes are possible), and the wide range of nanostructures that can be obtained (from nanoparticles, nanorods or nanoporous films, to nanowires) [11].

4.2. Hydrothermal/solvothermal

The hydrothermal/solvothermal method has also been widely used to prepare TiO_2 nanomaterials. In this case, the synthesis reaction is normally carried out in aqueous/organic solutions within steel pressure vessels called autoclaves under controlled temperature. The temperature can be raised above the boiling point of the water/organic solvent, reaching the pressure of vapor saturation. The temperature and the amount of solution added to the autoclave largely determine the internal pressure produced. The solvothermal method is almost identical to hydrothermal method except that the solvents used for solvothermal synthesis are non-aqueous, while water is the primary hydrothermal solvent. Consequently, the temperature in solvothermal process can be elevated much higher than that in hydrothermal method because a variety of organic solvents with high boiling points can be adopted. Normally, the solvothermal method possesses better control than hydrothermal methods over the size, structure, size distribution, and degree of crystallinity of TiO_2 nanoparticles [4].

In comparison with other methods, hydrothermal/solvothermal synthesis is a facile route to prepare a highly-crystalline oxide under moderate reaction conditions, such as low temperature (in general < 250^0C) and short reaction time. Meanwhile, it provides an effective reaction environment for the formation of nanocrystalline TiO_2 with high purity, good dispersion and well-controlled crystallinity. With this method, the sintering process, which results in a transformation from the amorphous phase to the crystalline phase, can be avoided. Similarly, by tuning the hydrothermal conditions (such as temperature, pH, reactant concentration and molar ratio, and additives), crystalline products with different composition, size and morphology can be achieved.

4.3. Electrochemical anodization

The controlled oxidation of titanium metal under electrochemical anodization provides another means of TiO_2 nanomaterial production. This technique is specifically amenable to the synthesis of TiO_2 nanotubes from titanium foil, which has been extensively studied after pioneering work in 2001 by Gong and co-workers, in which they reported the formation of nanotubes up to 0.5 mm length by electrochemical anodization of titanium foil in HF aqueous electrolyte [78]. The anodization of titanium is generally conducted in a two-electrode electrochemical cell at a constant potential in aqueous or organic electrolyte containing F^- with platinum foil as a cathode. Normally, the anodization process can be roughly divided into three stages: (1) the electrochemical oxidization of the titanium surface results in the formation of an initial TiO_2 barrier layer, corresponding to the first current drop, (2) TiO_2 is chemically etched by F^- to form TiF_6^{2-}, resulting in nanotube formation that leads to a current increase, and (3) the growth of nanotubes relates to a slow current decrease. Briefly, the nanotube growth is determined by the equilibrium between anodic oxidation and chemical dissolution. The anodic oxidation rate is mainly controlled by the anodic potential, while the chemical dissolution rate is greatly governed by the electrolyte acidity and F^- concentration [79-82].

Compared to other methods, anodic oxidation is a relatively simple technique that can be easily automated for the preparation of TiO_2 nanotube arrays with highly ordered structure and controllable size, which is mainly determined by the applied anodic potential, electrolyte composition, temperature, and time. Moreover, under optimized conditions, it also feasible to prepare other TiO_2 nanoarchitectures, such as nanorods and mesoporous structures [4].

4.4. Physical/chemical vapor deposition

Vapor deposition describes a procedure in which materials in a vapor state are condensed to form a solid phase material, and the whole process is usually conducted within a vacuum chamber. If no chemical reaction occurs, this process is called physical vapor deposition (PVD), otherwise it is called chemical vapor deposition (CVD) [4,15]. In PVD, materials are evaporated and subsequently condensed to form a solid material. The primary PVD methods include thermal deposition, ion plating, ion implantation, sputtering, laser vaporization, and laser surface alloying [4,15]. However, in CVD processes, thermal energy heats the gases in the coating chamber to induce a deposition reaction. Typical CVD approaches include electrostatic spray hydrolysis, diffusion flame pyrolysis, thermal plasma pyrolysis, ultrasonic spray pyrolysis, laser-induced pyrolysis, atmospheric pressure, and ultrasonic-assisted hydrolysis

[4,15,31,83]. Several TiO_2 nanostructures prepared though PVD or CVD have been reported. For example, TiO_2 nanoparticles with sizes below 10 nm were prepared by pyrolysis of TTIP via a CVD process in a mixed helium/oxygen atmosphere [84]. TiO_2 nanorods were grown on a Si substrate using TTIP as the precursor by metal organic CVD (MOCVD) [85], and aligned TiO_2 nanowire arrays were fabricated onto Si wafers by a simple thermal deposition (PVD) method [86].

4.5. Chemical (template) deposition

Templated synthesis of nanostructured materials has become extremely attractive during the last decade. This method utilizes the morphological properties of known and characterized templates in order to assemble materials with a similar morphology by reactive deposition or dissolution methods. By adjusting the morphology of the template material, it is possible to prepare numerous new materials with a regular and controllable morphology on the nano- and micro scale. One of the most commonly used templates, an alumina membrane having uniform and parallel porous structures, is prepared by anodic oxidation of aluminum sheets in solutions of sulfuric, oxalic, or phosphoric acids [11]. Many TiO_2 nanostructures have been achieved through template assisted deposition processes. For instance, large-area free-standing arrays of TiO_2 nanorods and nanotubes were selectively synthesized on transparent conducting indium tin oxide (ITO) substrates using anodic alumina (AAO) thin film templates [87], highly oriented TiO_2 nanotubes have also been fabricated using ZnO nanorod template through liquid reactive deposition on the ITO substrates [88].

The template approach is suitable for preparing nanoarrays of materials that are difficult to produce by other solution techniques. Nevertheless, in most cases, the template material is sacrificial and needs to be removed after synthesis, leading to an increase in the cost of materials. As in the case of all surface-finishing techniques, it is important to maintain a high level of surface cleanliness to ensure good adhesion between the template and the surface coating.

It is worth noting that in practice, novel morphologies are often obtained using a combination of two or three methods. For example, TiO_2 nanoparticles and films can be obtained by treating titanium isopropoxide with water, followed by hydrothermal post-treatment [89,90], or electrochemical oxidation together with sol treatment [91].

5. TiO_2 nanoarchitectures

A large internal surface area is the foremost requirement for the photoinduced reactions in DSSCs, water splitting, and organic chemical photocatalysis. Nanomaterials can satisfy this criterion because the specific surface area of nano-scale morphologies may be more than 1000 times greater than bulk materials. In an effort to enhance photocatalytic efficiency, various architectures of nanostructured TiO_2 have been investigated including nanoparticles, nanorods, nanowires, and nanotubes. In this section, a series of nanostructured TiO_2 architectures are discussed. An effort is made to summarize typical synthesis procedures for each structure, and representative transmission or scanning electron microscopy images are provided to give the reader an appreciation for the variety of nanoarchitectures currently available.

5.1. TiO_2 nanoparticles

In the past decade, the number of literature articles about nanostructured TiO_2 materials has increased considerably. Particularly, nanoparticle TiO_2 thin films have attracted great attention, partially due to the high surface area to volume ratio afforded by numerous surface-active sites, the direct availability of porous structures with assembled nanoparticles for electrolyte infiltration, and the simplicity of manufacturing films using chemically based solution methods [69]. One commercial form of TiO_2 nanoparticles, Degussa P25, is a standard industrial photocatalyst prepared by the hydrolysis of $TiC1_4$ in pure water or a 1:1 EtOH-H_2O solution. The relatively short residence time necessary for the conversion of $TiCl_4$ to TiO_2 gives a product which has a high surface area (~50 m^2g^{-1}) and phase mixture of approximately 4:1 anatase to rutile [2,63]. However, for a specific photoinduced reaction system, it is desirable to optimize the particle size and crystal phase as well as select a suitable synthesis method. This has prompted the development of several experimental procedures for preparing TiO_2 nanoparticles as well as theoretical strategies for structure prediction [25,34,92-96].

TiO_2 nanoparticles have been extensively prepared by the sol-gel method. Numerous research efforts have shown that various parameters related to the sol-gel process have a great impact on both the TiO_2 nanoparticle phase and average particle sizes [32,36,89,90,97-101]. For example, it was found that decreasing the Ti/H_2O molar ratio resulted in both decreasing brookite content and anatase particle size in sol-gel synthesized TiO_2

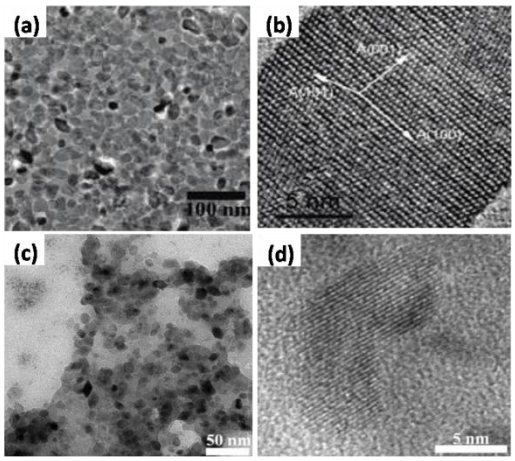

Figure 6. TEM (a, c) and HR-TEM (b, d) images of the TiO_2 nanoparticles prepared by sol-gel process. (Reprinted with permission from Reference [75] (a) and (b): Lee, S. et al., Chem. Mater. 2010, 22, 1958-1965. Reference [89] (c) and (d): Isley, S. L. et al., J. Phys. Chem. B 2006, 110, 15134-15139. Copyright © American Chemical Society).

nanoparticles [89]. In addition, hydrothermal aging, a common post-treatment for sol-gel synthesis, has several tunable variables such as pH [90], dialysis [89], and temperature [89], which have been proven to influence particle growth and relative phase stability. However, the products of hydrothermal aging depend most strongly upon the initial phase composition and average particle sizes after sol-gel synthesis, which are most sensitive to the pH employed during sol-gel synthesis. Therefore, substantial control over the brookite content, particle size, and particle growth mechanism can be achieved simply by changing the pH of the sol and gel [90]. Furthermore, the growth kinetics of TiO_2 nanoparticles synthesized from sol-gel processes has been investigated. It was demonstrated that the aggregation kinetics of TiO_2 nanoparticles was influenced by the ionic strength and pH of suspensions and the nature of the different cation valences present in the electrolyte [97,102], yet, the average particle radius increased linearly with time in agreement with the Lifshitz-Slyozov-Wagner model for coarsening, where the rate constant for coarsening elevated with temperature [98].

It is worth noting that although the conventional sol-gel process is capable of large-scale production, it is incapable of producing TiO_2 nanoparticles with controlled shape and size distributions. Accordingly, a novel two-step sol-gel process has been developed to synthesize uniform TiO_2 nanoparticles. In this method, oxide particles are grown via two steps: (1) the formation of a hydroxide gel and (2) nucleation and growth of oxide particles. This process is distinguishable from the conventional sol-gel method, in which the gel phase develops first and is converted to a sol phase. The two-step sol-gel process is based on the idea of using a highly condensed precursor metal hydroxide gel as a protective matrix against coagulation of the growing particles as well as a reservoir of metal ions. With this strategy, TiO_2 nanoparticles of uniform size distribution and various shapes can be obtained, and anatase nanoparticles synthesized this way were shown to possess high crystallinity, size uniformity, negligible surface defects, and negligible residual organic compounds, all of which are beneficial properties for photovoltaic applications (see Figure 6). When organized into a DSSC sensitized by N719 dye, the photoanode exhibited a much higher efficiency (6.72%) than that of the P25 TiO_2 (4.0%) because of enhanced dye adsorption and charge transport [75].

It is well documented that TiO_2 nanoparticles can also be prepared by hydrothermal procedures. The influence of various hydrothermal parameters on the formation, phase, morphology, and grain size of products have been investigated and discussed in many published reports [36,76,103-109]. In general, the particle growth kinetics under hydrothermal conditions is believed to be determined by coarsening and aggregation–recrystallization processes, allowing control over the average nanoparticle size [110,111]. For instance, pure phase TiO_2 nanoparticles in anatase, rutile and brookite structures as well as their mixtures were fabricated using amorphous TiO_2, titanate alkoxide, or halide salts as precursors [104,105,110,111]. Particles of different phases could be achieved by hydrothermal treatment at elevated temperatures and suitable pH values with the appropriate reactants [110,111]. Anatase nanoparticles were obtained using acetic acid, while pure rutile and brookite nanoparticles were obtained with hydrochloric acid at a different concentration

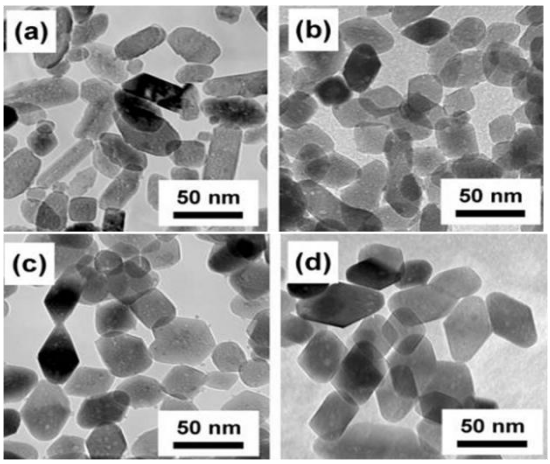

Figure 7. TEM images of TiO_2 nanoparticles prepared by hydrothermal process in different conditions.(Reprinted with permission from Reference [106] ' Murakami, N. et al., J. Phys. Chem. C 2009, 113, 3062-3069. Copyright © American Chemical Society).

[111], rutile precipitation at low pH and anatase growth at high pH were promoted [110]. It was proposed that anatase formation was dominated by surface energy effects, while the formation of rutile and brookite acted in a dissolution–precipitation mechanism, where chains of six fold-coordinated titanium complexes gathered into different crystal structures [111]. Particularly, anatase TiO_2 particles with specific exposed crystal faces could be prepared by hydrothermal treatment of peroxo titanic acid (PTA) solution with polyvinyl alcohol as a shape-control reagent. TiO_2 particles prepared from a PTA solution of pH 7 had (101) and (001) exposed crystal faces, which showed higher photocatalytic activity for acetaldehyde decomposition than commercial spherical TiO_2 particles, and the shape of TiO_2 particles changed with the time of hydrothermal treatment (see Figure7) [106].

Besides sol-gel and hydrothermal methods, other common synthesis techniques have been applied to prepare TiO_2 nanoparticle films. For instance, recently, a novel and facile method termed phase-separation-induced self-assembly was developed to prepare TiO_2 nanodots with tunable size (28~93nm) and density ($4.05 \times 10^{10} \sim 0.45 \times 10^{10}$ cm^{-2}) on a substrate (see Figure 8), and it was found that smaller nanodots exhibited a pronounced hydrophilic characteristic with improved wettability due to an increase in solid–liquid area. This method induced convective flow in a spin-coated titanium tetrabutoxide (TBOT)/polyvinyl pyrrolidone (PVP)/ethanol liquid film through the Marangoni effect.

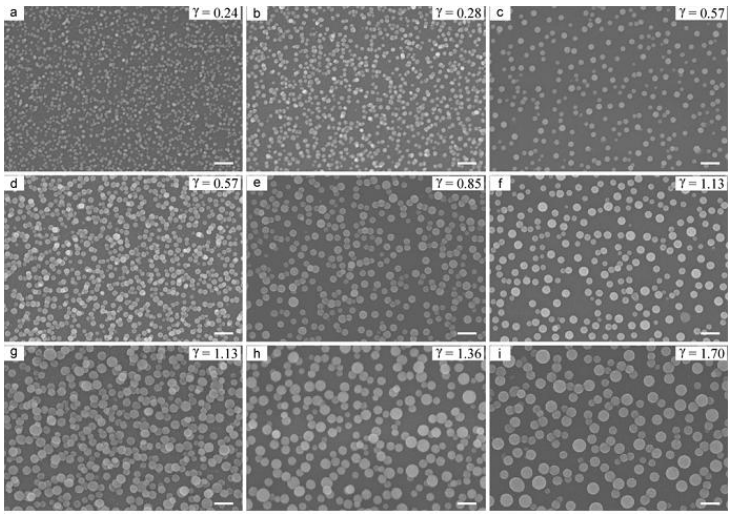

Figure 8. SEM images of TiO_2 nanodots with different morphologies prepared on silicon substrates (bar represents 200 nm). (Reprinted with permission from Reference [112] , Luo, M. et al., Nanotechnology 2009, 20. Copyright © IOP Publishing).

Subsequent calcination transformed TBOT into crystalline TiO_2 nanodots on the substrate [112]. Another femtosecond and nanosecond pulsed laser deposition (PLD) technique at different laser wavelengths has been widely used to construct nanoparticle-assembled TiO_2 films. This technique allows for control of the dimensions and crystalline phase of nanoparticles by varying the laser parameters, and the deposition conditions and suitable for depositing TiO_2 films at a relative high rate and low cost [113-115].

The most efficient (~11% PCE) TiO_2 electrodes in DSSCs use 10-μm-thick TiO_2 nanoparticle films consisting of an interconnected network of nanometer-sized crystals ~20 nm in diameter [61]. It has been confirmed that this type of structure imparts sufficient surface area to adsorb a large amount of dye molecules, leading to efficient light absorption and charge formation [116-118]. The effects of particle size on the overall performance of DSSCs have been investigated. Larger particle-based films have larger contact points between sintered colloidal particles and at the interface between the particles and the underlying substrate. The relatively small number of grain boundaries beneficially improves charge transport, though the small surface area deleteriously limits dye adsoprtion. Smaller particle-based films provide a larger surface area together with a greater number of contact points between sintered colloidal particles and between particles and the underlying substrate. The large surface area allows for greater dye adsorption, but the increased number of contact points reduces charge mobility by increasing electron trapping events [117,119,120]. The mechanisms of particle size effect on electron injection efficiency in ruthenium dye-sensitized TiO_2 nanoparticle films were investigated by using time-resolved fluorescence spectroscopy and femtosecond (transmittance and diffuse reflectance) transient absorption spectroscopy. It was found that small diameter systems gave high electron injection yields (around 90%), whereas larger diameter systems gave low efficiencies (from 35 to 70%). The dye loading of the larger diameter systems was greater than that of small diameter systems because more than a monolayer of dye adsorbed to the larger particles, which resulted in low efficiencies in the larger diameter systems. Importantly, the comprehensive and systematic time-resolved spectroscopic data pointed out that the dye aggregates formed in spaces between TiO_2 nanoparticles were the crucial factor for reducing electron injection efficiency rather than the size-dependent surface nature of TiO_2. In brief, for DSSC application, dye aggregation must be carefully treated and avoided in order to achieve high performance, especially when using larger semiconductor nanoparticles, which often work as a light-scattering material [120].

5.2. Mesoporous TiO_2

Mesoporous materials containing nanoparticles distributed throughout structures of adjustable pore size and high specific surface area have attracted considerable interest during the past decade. In particular, mesoporous TiO_2 materials with tailored pore size, high specific surface area, and well-defined crystalline configuration have potential applications in solar cells, photocatalysis, and water splitting. Importantly, the pore size and specific surface area of mesoporous TiO_2 materials greatly influences their physical properties related to photocatalytic activity. For instance, in catalytic applications, a tunable pore size can facilitate the diffusion rate of reactants toward adsorption sites, while a high surface area can maximize the interface between the reactants and the catalyst surface. For DSSCs, mesoporous TiO_2 can enhance light harvesting within the electrodes without sacrificing the accessible surface for dye loading [121-123].

When prepared via sol-gel methods, the pore size of mesoporous TiO_2 can be tuned by addition of a structure-directing agent with different hydrophobic chain lengths (e.g., triblock copolymer, Pluronic F127) or by addition of a swelling agent (e.g., mesytilene), which can be removed either by calcination in air or by reaction with a solvent when the synthesis procedure is completed. However, the specific surface area is determined mostly by the hydrolysis ratio. Usually, a high water/alkoxide ratio enables a more complete hydrolysis of the titanate alkoxide precursor, supporting nucleation instead of particle growth and leading to small particles with high specific surface areas [121,124,125]. The sol-gel process using organic surfactants as assisting templates represents the most widely used route for the synthesis of mesoporous TiO_2 and involves a complicated mechanism called evaporation-induced self-assembly (EISA). The EISA process produces an ideal grid-like morphology consisting of a continuous, ordered network of anatase TiO_2 with a high surface area by condensation of a titanium precursor around self-organized organic templates in a gel phase, followed by removal of the templates. With this method, electrodes can be prepared directly on Si or FTO substrates. Furthermore, the process is highly scalable because it can be performed at low temperature without any expensive or complicated equipment [121,122,126,127]. For example, ordered

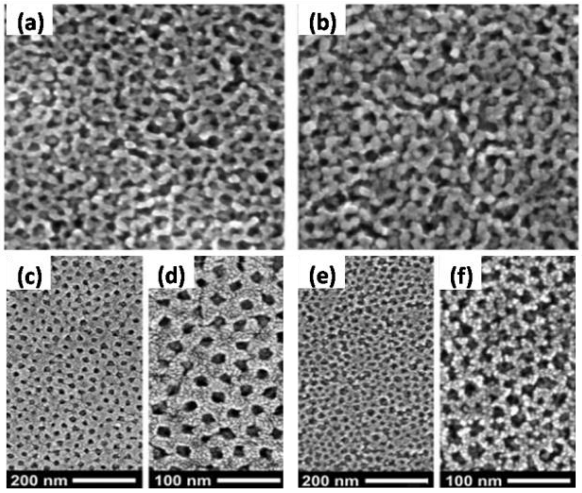

Figure 9. SEM images of mesoporous TiO_2 films. (Reprinted with permission from Reference[125] (a)~(b): Zukalova, M. et al., Nano Lett. 2005, 5, 1789-1792. Reference [126](c)~(f): Hartmann, P. et al., Acs Nano 2010, 4, 3147-3154. Copyright © American Chemical Society).

mesoporous TiO_2 nanocrystalline films prepared via layer-by-layer deposition with Pluronic P123 as a template (see Figure 9) exhibited enhanced solar conversion efficiency with a remarkable enhancement of the short circuit photocurrent due to the large surface area accessible to both the dye and the electrolyte [125]. Pluronic P123 was also employed in another work as a template to attain optimized pore morphology, high crystallinity, and stable mesoporous TiO_2 films. These films were then modified by adding P25 nanoparticles that acted as scattering centers and functioned as active binders to prevent the formation of microcracks. The combination of increased surface area, light-scattering particles, and high crystallinity of the mesoporous films successfully enhanced the performance of DSSCs [124]. In another approach for the synthesis of mesoporous TiO_2, a simple method without organic structure-directing agents or pretreated substrates was developed to produce anatase TiO_2 through a reaction-limited aggregation in boric acid solution. The hydrolysis rate along with the motion of the TiO_2 nanoparticles could be controlled by adjusting the concentration of boric acid. A solar cell based on this mesoporous TiO_2 possessed high surface area, which increased dye loading and, subsequently, improved both photocurrent and cell efficiency [128].

Mesoporous TiO_2 can also be obtained though other procedures. For example, porous anatase TiO_2 films on stainless steel substrates were fabricated with $Ti(OC_4H_9)_4$ as a precursor via a hydrothermal process. The degree of crystallinity and porosity of the films were determined by the time and temperature of the hydrothermal reaction, and the resultant TiO_2 films showed high photocatalytic activity towards degradation of gaseous formaldehyde [129]. Furthermore, a thick self-organized mesoporous TiO_2 layer was grown on titanium foil by anodization in an organic/K_2HPO_4 electrolyte followed by chemical etching of the structure. This material, which consisted of a strongly interlinked network of nanosize TiO_2, provided a considerably higher specific surface area than TiO_2 nanotubes, and displayed enhanced conversion efficiency as an electrode in DSSCs after undergoing a $TiCl_4$ hydrolysis treatment (see Figure 10) [130].

5.3. TiO_2 microspheres

It is well known that, in spite of the large surface area of the TiO_2 nanoparticle-based film, it often suffers from having a disordered morphology with many grain boundaries, which gives rise to interfacial interferences to electron transport. Moreover, when using typical 10–20 nm-sized TiO_2 nanoparticles, the sizes are so much smaller than the wavelength of visible light that the film is transparent with little light scattering, which leads to poor light harvesting [131]. Accordingly, in order to satisfy the requirements for fast electron transport and high surface area along with enhanced light-scattering in thin-film photoelectrodes, spherical (or bead-like) TiO_2 with a submicrometer-sized diameter is under intense study for its relatively high refractive index and particle sizes, which are comparable to the wavelengths of optical light [132-134]. Sub-micrometer-sized TiO_2 spheres have often been prepared using sol–gel methods by controlling the hydrolysis and condensation reactions, followed by subsequent calcination to form crystallized structures. Monodispersed spherical TiO_2 structures can be successfully obtained by this procedure, but their low surface

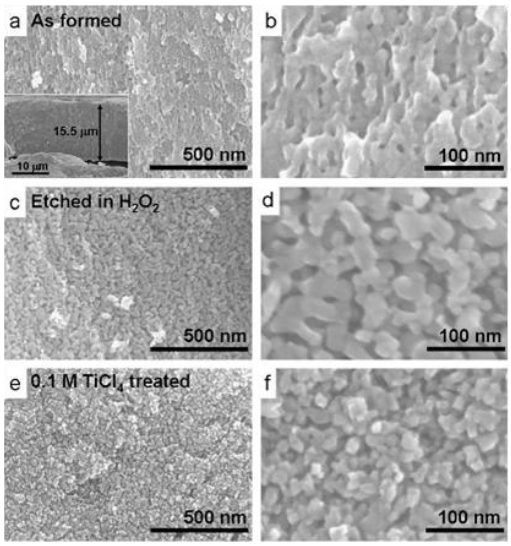

Figure 10. Cross-sectional SEM images of TiO_2 mesosponge formed on Ti by anodization in 10 wt% K_2HPO_4 in glycerol at 180 ± 1 ^{0}C as-formed (a, b), after etching in 30 wt% H_2O_2 for 1 h (c, d), and after treatment of the TiO_2 mesosponge in 0.1 M $TiCl_4$ (e, f). (Reprinted with permission from Reference [130], Kim, D. et al., Electrochem. Commun. 2010, 12, 574-578. Copyright © Elsevier).

area and poor pore structure impede widespread application [135,136].

To overcome the low surface area of microspheres as a result of smooth surfaces, some post-synthesis treatments (commonly solvothermal in nature) have been developed to produce special morphologies, including mesoporous microspheres and hollow microspheres [137]. For instance, crystalline mesoporous TiO_2 beads with surface areas up to 108.0 m^2g^{-1} were synthesized through a facile combination of sol-gel and solvothermal processes (see Figure 11). Due to their submicrometer-sized particle diameters and high specific surface areas, the mesoporous TiO_2 beads can enhance light harvesting in electrodes without sacrificing the amount of accessible surface area for dye loading, thereby increasing the conversion efficiency of DSSCs created with post-synthesis treated NPs (7.20%) compared to P25 nanoparticles (5.66%) [132]. Similarly, after the synthesis of sub-micrometer-sized TiO_2 spheres by sol–gel methods, a specially designed solvothermal treatment was employed instead of the conventional calcination process to develop crystallized nanoporous TiO_2 spheres with ultrahigh surface area and well-developed nanopore structure, which yielded an enhanced performance in DSSCs [135]. Recently, mesoporous TiO_2 beads were synthesized using a sol-gel process in the presence of hexadecylamine, following by solvothermal treatment in an ethanol-water mixture containing ammonia. When serving as the electrodes of

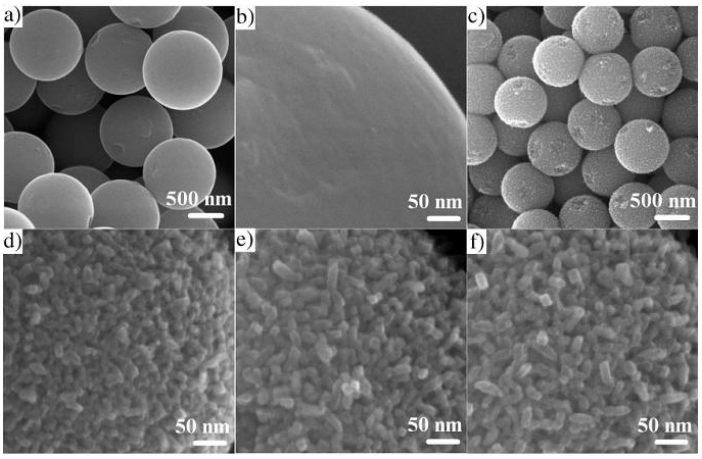

Figure 11. SEM images of the precursor material (a, b), and the mesoporous TiO_2 beads obtained after a solvothermal process with different amounts of ammonia (c, d, e, f). (Reprinted with permission from Reference [132], Chen, D. H. et al., Adv. Mater. 2009, 21, 2206. Copyright © Wiley-VCH).

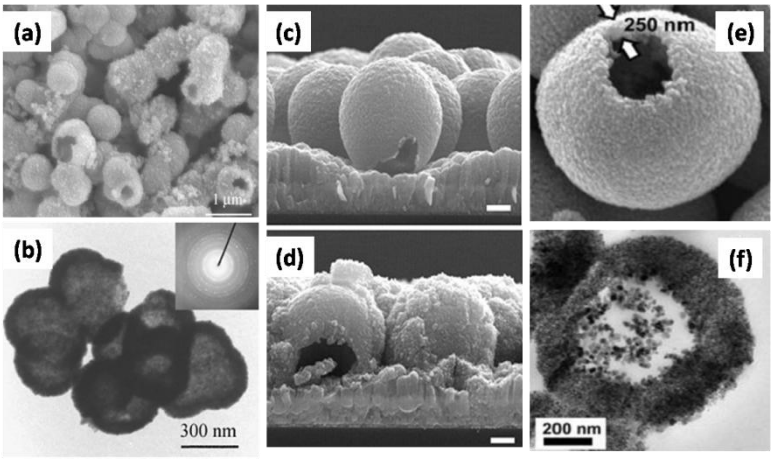

Figure 12. SEM (a, c, d, e) and TEM b, f) images of TiO_2 hollow microspheres. (Reprinted with permission from Reference [140] (a) and (b): Yu, J. G. et al., Adv. Funct. Mater. 2006, 16, 2035-2041. Reference [141] (c) and (d): Yang, S. C. et al., Adv. Mater. 2008, 20, 1059. Reference [139] (e) and (f): Kim, Y. J. et al., Langmuir 2007, 23, 9567-9571. Copyright © American Chemical Society and Wiley-VCH).

DSSCs, the as-prepared mesoporous TiO_2 beads demonstrated longer electron diffusion lengths and extended electron lifetimes over Degussa P25 electrodes due to the well interconnected, densely packed nanocrystalline TiO_2 particles inside the beads, which led to an enhanced power conversion efficiency (PCE) of greater than 10% [134].

In another approach, mesoporous anatase spherical TiO_2 architectures with high surface areas of up to 116.5 m^2g^{-1} were constructed by a simple urea-assisted hydrothermal process and investigated as dye-sensitized solar-cell electrodes. The DSSCs showed enhanced light harvesting and a larger amount of dye loading, which produced a significantly higher overall light conversion efficiency of 7.54% compared to a commercial Degussa P25 TiO_2 nanocrystalline electrode (5.69%) [133]. Meanwhile, highly-crystallized mesoporous TiO_2 microspheres with surface areas of up to 193.0 m^2g^{-1} were also created by hydrothermal treatment of the titanium diglycolate precursors and assembled into DSSCs with a high light-to-electricity conversion of 8.20%, indicating a 40% increase in the conversion efficiency compared to the standard Degussa P25 photoanode [131] Furthermore, mesoporous TiO_2 sub-microspheres with a size distribution from 80 nm to 3 μm were prepared using aerosol techniques with a non-equilibrium density gradient [136].

Micrometer-sized hollow spheres of TiO_2 nanocrystals have the beneficial properties of a large surface area, mesoporous morphology on both external and internal surfaces, which offers unique optical properties for light trapping and scattering despite the large size of the spheres [138-143]. For example, robust and size-controllable hollow TiO_2 microspheres (see Figure 12) constructed through the assembly of 18 nm TiO_2 nanoparticles have been synthesized via a solvothermal reaction of titanium isopropoxide by altering the concentration of tetrabutylammonium hydroxide to control their diameter. This technique is simple, highly reproducible, and amenable to low cost, large-scale synthesis [139]. Hollow TiO_2 microspheres can also be attained though a hydrothermal process with $TiOSO_4$ aqueous solution as a precursor (see Figure 12) [140]. Moreover, TiO_2 hollow spheres can be fabricated via a hydrothermal method using carbon spheres as hard templates through template-directed deposition, followed by calcination in order to remove the templates. The resulting TiO_2 hollow spheres exhibited superior photocatalytic activity for the degradation of Rhodamine B, 2.9 times greater than that of Degussa P25 [142]. Additionally, novel hollow TiO_2 hemispheres were produced through a combination of chemical and physical synthesis routes, namely, using a colloidal templating technique combined with an RF-sputtering method (see Figure 12). The hollow structure aided in electron transport, provided a large surface area for enhanced dye loading, and allowed penetration of even viscous electrolytes. When formed into TiO_2 photoanode films for DSSCs, the properties of these particles were found to enhance photoconversion efficiency [141].

Microsphere TiO_2 configurations comprised of 1D or 2D TiO_2 building blockings, such as nanorods, nanotubes or nanosheets have been fabricated [144-148]. For instance, single-crystalline rutile TiO_2 microspheres with diameters ranging from 0.65 to 2.5 μm were prepared by means of the assembly of 1D nanorods with diameters of 10–15 nm and shortest lengths of 250 nm through a simple

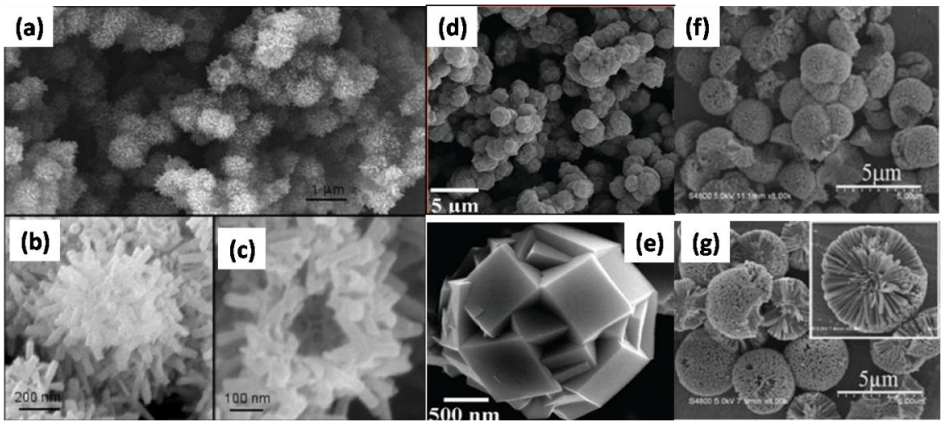

Figure 13. SEM images of TiO_2 hollow microspheres based on (a), (b), (c) nanotubes; (d), (e) nanosheets; (f), (g) nanorods. (Reprinted with permission from Reference [147] (a), (b) and (c):Tan, Y. F. et al., Langmuir 2010, 26, 10111-10114. Reference [145] (d) and (e): Zhang, H. M. et al., Chem. Commun. 2010, 46, 8395-8397. Reference [148] (f) and (g): Sang, Y. et al., Nanoscale 2010, 2, 2109-2113. Copyright © American Chemical Society and Royal Society of Chemistry).

surfactant-assisted solvothermal process in the presence of the surfactant Span 80 [146]. Recently, the fabrication of a microsphere-like TiO_2 architecture consisting of rutile nanorods with (110) exposed facets (see Figure 13) through a simple hydrothermal method without the use of templates was reported. A novel outside-in ripening mechanism was proposed to explain the formation of these TiO_2 architectures [148]. Moreover, hollow microspheres constructed of TiO_2 nanotubes were obtained via a hydrothermal process in a mildly alkaline solution, where the titanate nanotubes were formed by rolling sheets with the assistance of H_2O_2 (see Figure 13) [147]. Anatase TiO_2 microspheres with exposed mirror-like plane (001) facets (see Figure 13) were synthesized via a facile hydrothermal process. The photoanode composed of the as-formed TiO_2 microspheres showed an improved DSSC efficiency owing to the superior light scattering effect of microspheres and excellent light reflecting ability of the mirror-like plane (001) facets [145].

5.4. TiO_2 nanosheets

Among the low-dimensional morphologies of TiO_2, particular interest is being devoted to TiO_2 nanosheets, which are classified as two-dimensional systems having a thickness of a few atomic layers. Suprisingly, these structures can be remarkably stable despite their low dimensionality. TiO_2 nanosheets exhibit novel physical and chemical properties because of their two-dimensionality, including very intense and sharp UV absorption and enlargement of the band gap energy [149-151]. For example, lepidocrocite structured (which has a close structural relationship with anatase) nanosheets, in which Ti ions are in a six fold coordinated configuration, were computed to be 0.18 eV per unit formula higher in energy compared to bulk TiO_2 [152]. These first principle calculations also predicted large anisotropy in physical characteristics such as optical, dielectric, and mechanical properties [150,152,153]. Another important function of TiO_2 nanosheets has been their role as precursors for the creation of other morphologies, such as tubelike, boatlike, and wirelike TiO_2 [154-156].

For example, well-ordered multilayer films of TiO_2 nanosheets were prepared on a quartz-glass substrate using the layer-by-layer deposition method, and their photocatalytic oxidation ability was evaluated by decomposition of gaseous 2-propanol and bleaching of methylene blue dye under UV light illumination. However, the photocatalytic oxidation activity decreased with increasing number of nanosheet layers, and the investigation of the photochemical reactions on the number of nanosheet layers revealed the behavior of carriers generated in multilayered systems. That is, migration of these carriers was primarily limited to the two-dimensional plane, and hopping between the nanosheets was substantially restricted [149]. Additionally, perpendicular TiO_2 nanosheet films were produced on a titanium metal sheet by hydrothermal treatment with aqueous urea. The large-area flat plane of the TiO_2 nanosheet, which was oriented vertically relative to the substrate, was considered to be thermodynamically stable, while the edge plane, which had a thickness of several nanometers, was expected to be thermodynamically unstable (see Figure 14). Therefore, a perpendicular TiO_2 nanosheet film is predicted to display superhydrophilicity without UV irradiation because the edge plane should contain a large number of defects or dangling bonds as a result of thermodynamic instability [157].

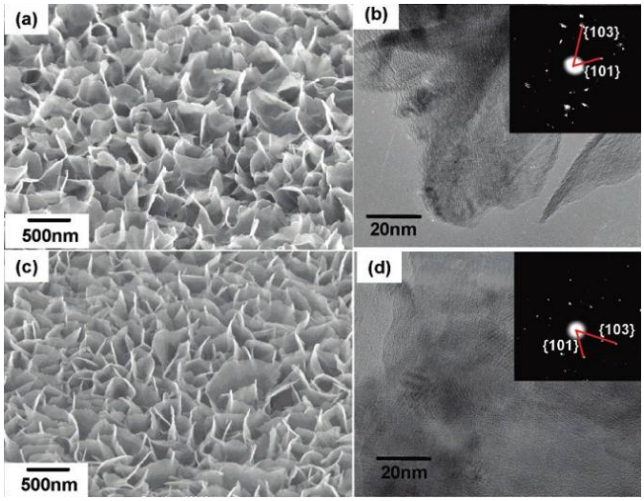

Figure 14. (a, c) SEM images and (b, d) TEM images of the perpendicular TiO_2 nanosheet films. (Reprinted with permission from Reference [157], Hosono, E. et al., Langmuir 2007, 23, 7447-7450. Copyright © American Chemical Society).

Experimentally, anatase TiO_2 nanosheets with largely exposed (001) facets have been synthesized [154,158], and theoretical studies have predicted that the (001) facets of anatase TiO_2 are much more reactive than the thermodynamically stable (101) facets. This prediction is based on the fact that (001) facets contain high densities of under-coordinated Ti atoms and very large Ti–O–Ti bond angles at the surface, and thus, the formed anatase nanosheets with exposed (001) facets exhibit a highly active photocatalytic effect [3,152,159]. For instance, anatase TiO_2 nanosheets, with dominant (001) facets fabricated by a facile hydrothermal route in a $Ti(OC_4H_9)_4$-HF-H_2O mixed solution, exhibited much higher photocatalytic activity in the photocatalytic degradation of acetone as well as enhanced performance of DSSCs compared to anatase TiO_2 nanoparticles with few (001) facets and Degussa P25 TiO_2 NPs (see Figure 15) [151,160].

5.5. TiO_2 nanotubes

Among the various forms of nanostructured semiconductors, One-dimensional (1-D) highly ordered architectures (such as nanowires, nanorods, nanobelts, nanoribbons, nanotubes) with high surface area-to-volume ratios possess useful and unique properties compared to that of their bulk counterparts. The highly orientated nature of these ordered 1-D nanostructures endows them with excellent electron percolation pathways for vectorial charge transfer between interfaces. For

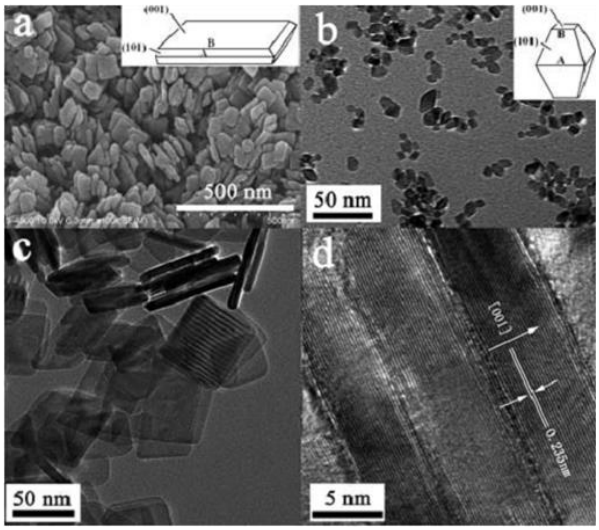

Figure 15. SEM (a), TEM (b and c) and HRTEM (d) images of TiO_2 nanosheets (a, c and d) and TiO_2-nanoparticles (b) films calcined at 450 ^{0}C. (Reprinted with permission from Reference [151], Yu, J. G. et al., Nanoscale 2010, 2, 2144-2149. Copyright © Royal Society of Chemistry).

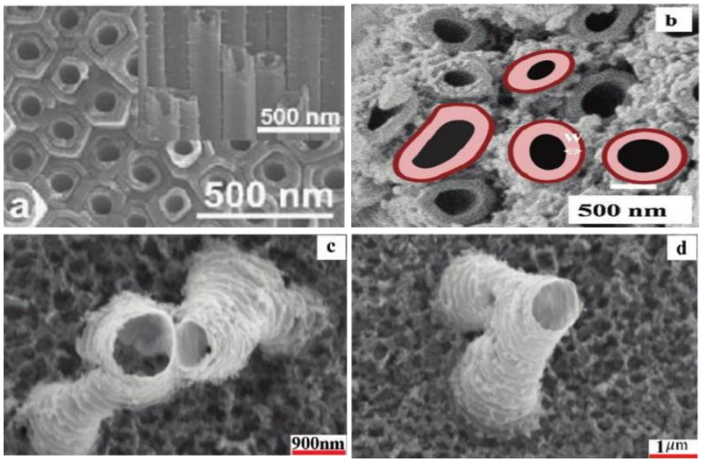

Figure 16. SEM images of (a) double-wall TiO_2 nanotubes; (b) large diameter TiO_2 nanotubes; (c) and (d) multipodal TiO_2 nanotubes. (Reprinted with permission from Reference [196] (a)Albu, S. P. et al., Adv. Mater. 2008, 20, 4135. Reference [198] (b): Yoriya, S.; Grimes, C. A. Langmuir 2010, 26, 417-420. Reference [197] (c), (d): Mohammadpour, A. et al., Acs Nano 2010, 4, 7421-7430. Copyright © Wiley-VCH and American Chemical Society).

example, the mobility of electrons in 1-D nanostructures is typically several orders of magnitude higher than that in semiconductor nanoparticle films [161-164]. In comparison with other 1-D morphologies, nanotubes provide a larger interfacial area due to their external and internal surfaces, which is beneficial for surface area dependent applications. Studies on TiO_2 have shown that vertically oriented nanotube arrays are remarkably efficient when applied in sensors, water splitting, dye-sensitized and solid-state solar cells, and photocatalysis [80,165-169].

TiO_2 nanotube arrays have been synthesized by a variety of methods, including template deposition (using nanoporous alumina templates, ZnO nanorod templates, or organo-gelator templates in sol–gel processes) [87,88,170-172], electrochemical anodization [79,81,173-175], and hydrothermal techniques [165,176-181]. Among them, the cheapest and most straightforward approach that leads to ordered nanotubes is the anodization method, which allows superior control over the resulting tube diameter, tube length, and overall morphology by the optimization of various parameters such as the pH, concentration, and composition of the electrolyte, as well as the applied potential, time, and temperature of anodization. That is, electrochemical anodization, in which the equilibrium between localized chemical dissolution with field-assisted oxidation and dissolution reactions takes place, produces precisely ordered nanoscale architecture by self-assembly [79,80,182].

Generally speaking, there are four development generations of nanotube arrays prepared by electrochemical anodization. The first report on the fabrication of highly ordered TiO_2 nanotube arrays was published in 2001 by Gong and co-workers, in which they reported the formation of nanotubes up to 0.5 mm length by electrochemical anodization of Ti foil in HF aqueous electrolyte [78]. This pioneering work began a decade-long effort to refine the novel technique, and a second generation of nanotube array synthesis was triggered by the subsequent work of Grimes and co-workers, in which the nanotube array length was increased to 6.4 μm by using an aqueous buffered electrolyte and by proper control of the anodization electrolyte pH to reduce chemical dissolution of the TiO_2 during anodization [79]. The third generation of TiO_2 nanotube array synthesis yielded nanotube lengths up to approximately 1000 mm using a non-aqueous, polar organic electrolyte (such as formamide, dimethyl sulfoxide, ethylene glycol, or glycerol) [183]. Recently, synthesis of TiO_2 nanotube arrays using non-fluoride electrolyte has been reported, which may be considered as the fourth synthesis generation [184,185].

To date, several reviews have illuminated the many aspects of synthesizing TiO_2 nanotube arrays through anodization [79-82]. By all accounts, the variation of experimental conditions can be used to tune the nanotube features [186-195], and double-walled TiO_2 nanotubes [196], multipodal TiO_2 nanotubes [197], large diameter TiO_2 nanotubes (see Figure 16) [198], and several other structures have been created. Regardless of structure, TiO_2 nanotube-based films must be optimized for use in DSSCs. TiO_2 nanotube arrays are commonly grown in situ on opaque titanium foils or sheets, but these are not suitable for achieving high-efficiency DSSCs because the incoming light is partially reflected by the counter electrode and partially absorbed by the counter electrode and iodine in the electrolyte

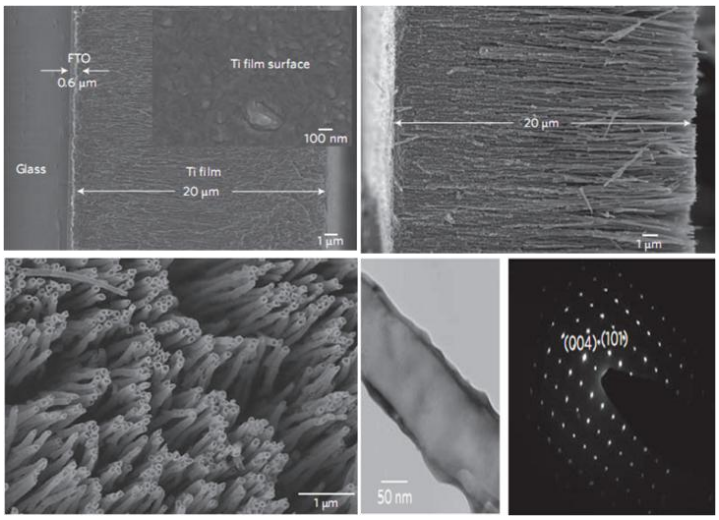

Figure 17. SEM images of (a) a 20-μm-thick Ti film deposited on FTO-coated glass. (b), (c) a 20-μm-long TiO_2 nanotube array from anodization of the as-deposited Ti film. (d) TEM image and selected area diffraction (SAD) pattern of a region of a TiO_2 nanotube fabricated from the as-deposited Ti film. (Reprinted with permission from Reference [199], Varghese, O. K. et al., Nat. Nanotechnol. 2009, 4, 592-597. Copyright © Nature Publishing Group).

before striking TiO_2 nanotubes, leading to a loss of ~25% of the incident solar energy [199]. Several strategies have been explored to circumvent this problem. One of the most straightforward solutions is to deposit titanium as a thin film on an adequate substrate (such as fluorine-doped tin oxide glass (FTO)) before anodizing it. This is usually performed by physical methods such as radio-frequency (RF) or direct-current (DC) magnetron sputtering [190,200-204]. Using such a deposition process, effective conversion of sputtered titanium into nanotube layers was achieved and DSSCs containing these arrays yielded a power conversion efficiency of 6.9% (see Figure 17) [199]. Another approach for getting TiO_2 nanotube arrays onto transparent conductive electrodes involves growing the array on titanium foil before transporting it to the electrode. In this method, a large-area free-standing TiO_2 nanotube film was grown and separated by a two-step anodization process before it was transferred onto FTO glass and anchored via a layer of TiO_2 nanoparticle paste [205-210]. However, in this case, the tube-ends at the bottom of the array were closed, and the interface between the TiO_2 nanotube arrays and the TiO_2 nanoparticle layer caused near-UV light absorption and front surface light reflection as well as blockage of the diffusion of redox reagents into the underlying TiO_2 nanoparticles coated on the collecting FTO substrate.

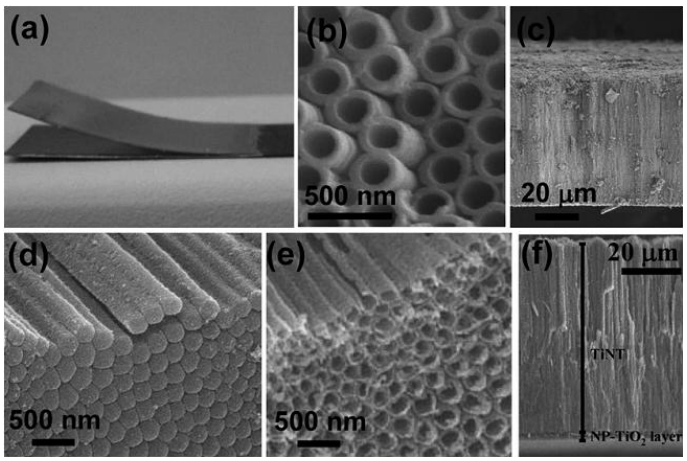

Figure 18. (a) Photograph and SEM images of (b) top, (c) side and (d) bottom views of the closed-end free-standing TiO_2 nanotube arrays; (e) and (f) SEM images of the opened-end free-standing TiO_2 nanotube arrays. (Reprinted with permission from Reference [211], Lin, C. J. et al., Mater. Chem. 2010, 20, 1073-1077. Copyright © Royal Society of Chemistry).

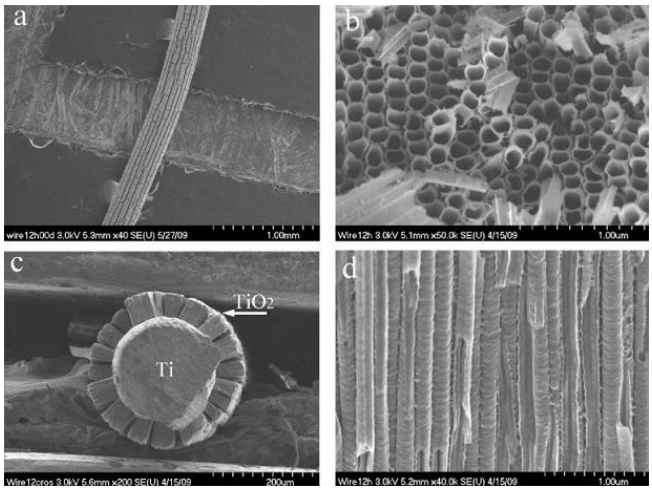

Figure 19. Top view (a, b) and cross-sectional (c, d) SEM images of TiO_2 nanotube arrays grown around a Ti wire fabricated by anodization at 60 V for 12 h. (Reprinted with permission from Reference [214], Liu, Z. Y.; Misra, M. Acs Nano 2010, 4, 2196-2200. Copyright © American Chemical Society).

Accordingly, the caps were removed from the closed bottom by immersing the as-prepared free-standing TiO_2 nanotube film in an oxalic acid solution. Compared to the closed-end TiO_2 nanotube-based DSSC, the opened-end TiO_2 nanotube-based device exhibited an increase in one-sun efficiency from 5.3% to 9.1%, yielding a 70% enhancement [211]. In addition to vertically aligned nanotubes, a novel version of DSSC, three-dimensional dye-sensitized solar cells (3D DSSCs), was introduced to overcome the light harvesting problem of TiO_2 nanotube-based electrodes. In this setup, titanium wires or meshes are utilized instead of titanium foils or sheets to fabricate TiO_2 anodized nanotubes [212-217]. For instance, Misra et al applied a TiO_2 nanotube-based wire as a working electrode (see Figure19) and platinum wire as a counter electrode in a DSSC, which achieved a conversion efficiency of 2.78% under AM 1.5 simulated sunlight. The prototype device was capable of achieving long distance transport of photocurrent and harvesting of light from any direction to generate electricity [214]. TiO_2 nanotubes were also directly grown on spiral-shaped titanium wire via anodization and assembled into a 3D DSSC coupling to a special platinized titanium wire counter electrode. Unlike conventional flat DSSCs, this 3D DSSC could easily hold liquid electrolyte due to capillary forces that facilitated sealing of the cell. These solar cells showed an enhanced energy conversion efficiency of 4.1% under the AM 1.5 condition compared with that (3.2%) of the backside illuminated TiO_2 nanotube-based DSSC having the same projected area [217]. Furthermore, Wang et al. developed a new type of 3D DSSCs with double deck cylindrical Ti meshes as the substrates. Here, one of the Ti meshes is anodized to synthesize the self-organized TiO_2 nanotube photoanode layer in situ. Another Ti mesh is platinized through electrodeposition as the counter electrode. This all-Ti solar cell exhibited the highest conversion efficiency for 3D DSSCs of 5.5% under standard AM 1.5 sunlight [213].

5.6. TiO_2 nanowires/nanorods

As mentioned above, 1-D TiO_2 nanocrystals have several advantages over their spherical counterparts for environmental and energy applications because of their high surface area-to-volume ratio and enhanced charge transport properties afforded by the decreased number of intercrystalline contacts and elongated structure. As important members of the 1-D structure family, the development of semiconductor nanowires/nanorods will provide an opportunity to understand the physical properties of all 1-D semiconductor nanomaterials and facilitate the realization of electrical, optical, and optoelectronic devices that employ nanowires/nanorods-based materials. TiO_2 nanowires and nanorods are of particular interest because of their demonstrated applications in a wide variety fields including DSSCs, water splitting, photocatalysis, and so forth [218-224].

As with the other TiO_2 structures, nanowires and rods can be synthesized by a broad set of methods including solvothermal/hydrothermal [37,38,225-230], chemical oxidation [77,231,232], sol-gel [233-235], and physical vapor deposition techniques [236-238]. For example, sol–gel processes enable the growth of anatase TiO_2 nanowires from FTO substrates, which are sensitive to a number of factors. The mechanisms of this reaction can be tentatively described as follows. First, Ti-oxide molecular clusters are bound to

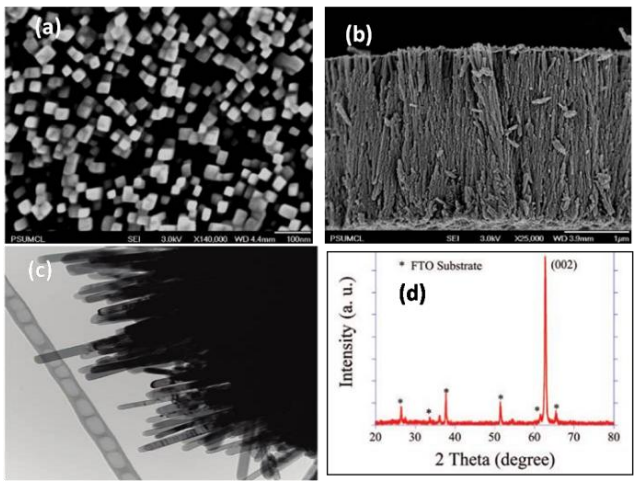

Figure 20. (a) and (b) SEM, (c) TEM images, and (d) XRD pattern of vertically oriented single crystal TiO_2 nanowire array grown on FTO coated glass. (Reprinted with permission from Reference [247], Feng, X. J. et al., Nano Lett. 2008, 8, 3781-3786. Copyright © American Chemical Society).

the pretreated FTO substrates, followed by a series of subsequent hydrolysis steps, which facilitate the axial growth of linear macromolecules normal to the plane of the FTO crystal faces. Calcination then produces a thin film of anatase TiO_2 nanowires tethered to the FTO surface [234]. TiO_2 nanorods were also synthesized via a sol-gel method utilizing Pluronic P-123 triblock copolymer, and the resultant nanorod-based DSSC showed improved performance with a Voc of 0.68 V, Jsc of 15.3 mA cm^{-2}, fill factor of 0.6, and efficiency of 6.2 %, due to the reduced intercrystalline contacts between grain boundaries and stretched structure, which facilitated greater electron transport than a similar NP-based DSSC (a Voc of 0.63 V, a Jsc of 10.9 mA cm^{-2}, a fill factor of 0.63, and an efficiency of 4.3%) [239]. In addition to solar cells, dense and aligned TiO_2 nanorod arrays have found utility as electrodes in PEC studies for hydrogen generation from water splitting. These structures were fabricated using oblique-angle deposition on indium tin oxide (ITO) conducting substrates, and overall water splitting was observed with an applied over potential at 1.0V (versus Ag/AgCl) with a photo-to-hydrogen efficiency of 0.1% [240]. Furthermore, rod-based TiO_2 anatase nanocrystals were made by a simple one-step solvothermal method, which prevented the formation of coarse aggregates and provided nanostructured films, in which the original shapes and sizes of the constituent nanorods were preserved. The as-prepared photoelectrodes showed a higher surface area and a better transparency with respect to those made with commercial P25 TiO_2, and the corresponding DSSCs exhibited a 16.9 $mAcm^{-2}$ photocurrent density with a conversion efficiency of 7.9% [241].

While 1-D polycrystalline TiO_2 nanostructures suffer from deleterious electron scattering or trapping at grain boundaries, the synthesis of aligned single-crystalline TiO_2 nanorod and nanowire films has attracted much attention because the resultant films could offer direct electrical pathways to increase the electron transport rate, which in turn may improve the performance of photovoltaic devices [33,225,242-245]. For example, the electron transport in single-crystalline nanowires is expected to be several orders of magnitude faster than percolation through a random polycrystalline nanowire network. In practice, DSSCs using single-crystalline anatase TiO_2 nanowire electrodes formed in a network structure by surfactant-assisted self-assembly processes exhibited a high conversion efficiency of 9.3% due to rapid electron transfer in the Nanowires [246]. Single crystal rutile TiO_2 nanowire arrays have also been grown vertically from a TCO glass substrate along the (110) crystal plane with a preferred (001) orientation via a solvothermal process and showed an AM 1.5 photoconversion efficiency of 5.02% in a DSSC (see Figure 20) [247]. Moreover, oriented single-crystalline rutile TiO_2 nanorod films grown on FTO substrates were developed by a facile hydrothermal treatment and achieved a conversion efficiency of 3% when used as the photoanode in a DSSC (see Figure 21) [244]. A versatile method for the synthesis of single-crystalline rutile phase TiO_2 nanowires on arbitrary substrates including FTO glass, glass slides, ITO glass, Si/SiO_2, Si (100), Si (111) and glass rods has been developed. However, optimization of the growth conditions only led to well-aligned vertical arrays of TiO_2 nanowires on both FTO and glass substrates. The application of vertical arrays of TiO_2 nanowires

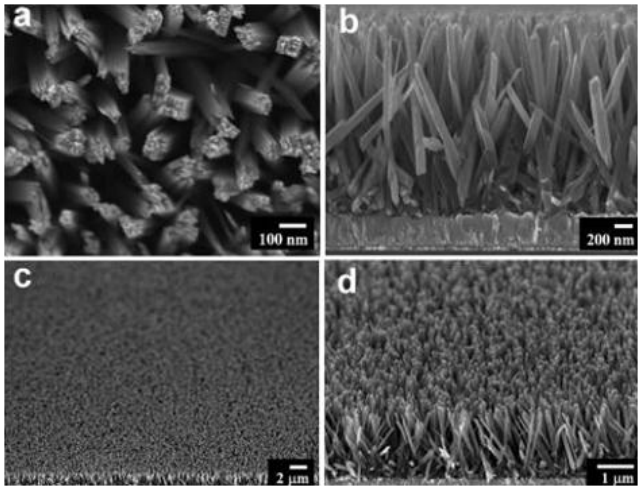

Figure 21. SEM images of oriented rutile TiO_2 nanorod film grown on FTO substrate (a) top view, (b) cross-sectional view, (c) and (d) tilted cross-sectional views. (Reprinted with permission from Reference [244], Liu, B.; Aydil, E. S. J. Am. Chem. Soc. 2009, 131, 3985-3990. Copyright © American Chemical Society).

on FTO as the photoanode in DSSCs was also demonstrated, and an efficiency of ~3.0% was achieved [243].

Recently, some colorful terms have been adopted to describe several special 1-D rod-like TiO_2 structures, such as nanofiber [248-253], nanospider [254], nanopillar [255-258], nanospindle [259-261], nanoframe [262], bipyramid [263], and rice-like (see Figure 22) TiO_2, [264,265]. TiO_2 nanofibers can be readily distinguished from TiO_2 nanowires and nanorods by their dimensions: nanowires and nanorods are structures with diameters of tens of nanometers, nanowires have undefined lengths, while nanorods typically have lengths in the range of ca. 1–100 nm. In contrast, electrospun nanofibers have diameters of 100 nm or larger and lengths of tens of microns or longer [248,252]. While the above definitions represent the most common application of the terms, these rules are frequently broken in the literature.

5.7. TiO_2 nanostructure transformation

Remarkably, under special synthesis conditions, all of the TiO_2 architectures can transform into each other. It is even possible to transform diversely shaped TiO_2 nanocrystals via a single synthesis method by adjusting experimental conditions [266-271]. For example, hydrothermally formed $Na_2Ti_6O_{13}$ nanostructures can be easily tuned by varying the experimental parameters of temperature, reaction duration, and

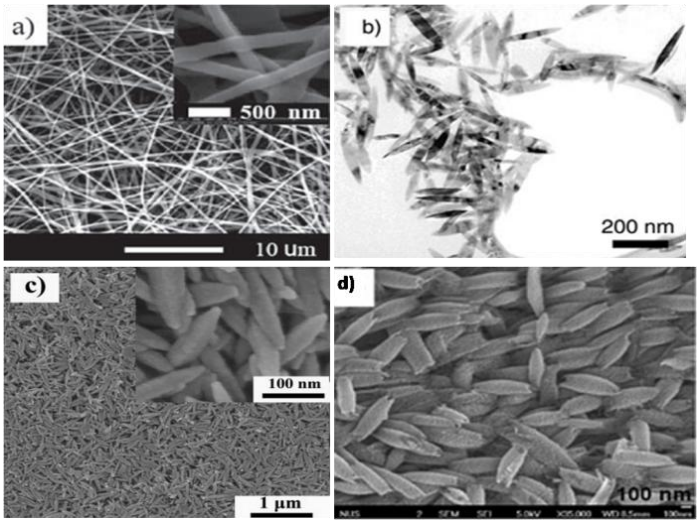

Figure 22. SEM images of TiO_2 (a) nanofibers; (b) and (c) nanospindles; (d) Rice grain-shaped. (Reprinted with permission from Reference [248] (a) Zhang, W. et al., Small 2010, 6, 2176-2182. Reference [259] (b) Qiu, Y. C. et al., Angew. Chem.-Int. Edit. 2010, 49, 3675-3679. Reference [261] (c) Qiu, Y. C. et al., Acs Nano 2010, 4, 6515-6526. Reference [264] (d) Nair, A. S. et al., Chem. Commun. 2010, 46, 7421-7423. Copyright © Wiley-VCH, American Chemical Society and Royal Society of Chemistry.

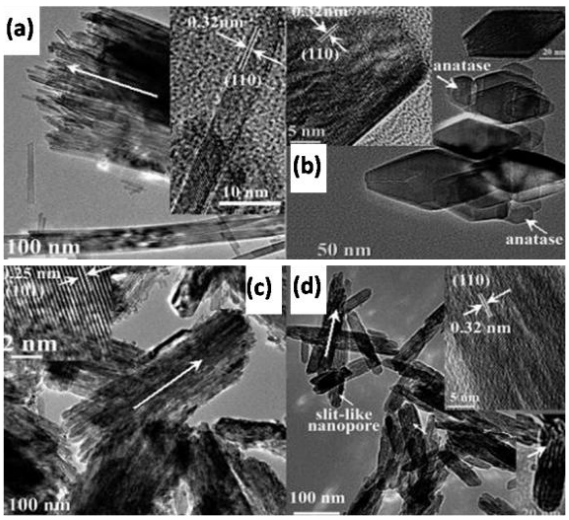

Figure 23. SEM and TEM images of TiO_2 (a) aligned rutile ultralong nanorods; (b) a mixture of diamond-shaped rutile and spherical anatase nanocrystals; (c) aligned rutile short nanorods; (d) porous rutile nanorods with slit-like nanopores. (Reprinted with permission from Reference [273], Shen, L. M. et al., J. Phys. Chem. C, 2008, 112, 8809-8818. Copyright © American Chemical Society).

NaOH concentration in order to obtain nanoplates, nanowires, and continuous nanowire network films. The shapes of the $Na_2Ti_6O_{13}$ nanostructures formed were preserved when converted into $H_2Ti_3O_7$ nanostructures by an ion-exchange process, which served as desirable precursors in the fabrication of corresponding TiO_2-based nanomaterials [272]. Again, a variety of TiO_2 nanostructures, including aligned nanorods, nanoporous nanostructures, nanocubes and diamond-shaped nanocrystals have been prepared through an inorganic, acid-assisted hydrothermal route, in which the nature and concentration of the inorganic acid (HCl, HNO_3,or H_2SO_4) determined the morphology, crystalline phase, composition, average grain size, band gap, and microstructure of the nanostructures (see Figure 23) [273]. Furthermore, TiO_2 nanostructures with controllable morphologies such as cubes, spheres, and rods were synthesized by a simple microwave irradiation technique. Transformation of different morphologies was achieved by tuning the pH and the nature of the medium or precipitating agent [274].

In addition to control of the synthesis parameters, there is another route for TiO_2 nanostructure transformation, that is, one kind of as-prepared architecture can be directly converted into another type of morphology via a post-synthesis treatment. In this respect, many transformations are possible, including rods to tubes [275], tubes to rods [276], tubes to particles [277-281], tubes to wires [282], etc. For instance, rutile TiO_2 nanorods prepared by the hydrolysis of titanium butoxide via a sol–gel process were hydrothermally treated using hydrochloric acid solution, which led to a novel morphology of rutile TiO_2 tapered nanotubes with rectangular cross-sections. A plausible anisotropic corrosion mechanism was proposed for this transformation [275]. In addition, hydrothermal treatment of TiO_2 nanotube suspensions under an acidic environment resulted in the formation of single-crystalline anatase nanorods with a specific crystal-elongation direction. The nanotube suspensions were prepared by a hydrothermal treatment of P25 TiO_2 nanoparticles in NaOH solution, followed by mixing with HNO_3 [276]. Interestingly, the conversion from nanotubes to nanoparticles can be performed via treatment of the as-anodized TiO_2 nanotubes in concentrated aqueous ammonium hydroxide solution prior to calcination at elevated temperatures [280], through a thermal annealing of the as-anodized TiO_2 nanotubes in ambient fluorine resulting from the electrolyte residues of anodization [277,279,281], or by a 180^0C hydrothermal process of the as-anodized TiO_2 nanotubes placed on a support to avoid direct contact with the water in the reaction container (see Figure 24) [278].

5.8. TiO_2 nanostructure combinations

Since every structure discussed thus far possesses unique properties (such as the high surface area of nanoparticles and high electron mobility and transport rate of 1-D architectures), the combination of two or more structures holds promise to synergistically improve the performance of photocatalytic devices. Several combinations have attracted interest including nanotube/ nanoparticle [283-286], nanorod/ nanoparticle [21, 30, 287-289], nanowire /

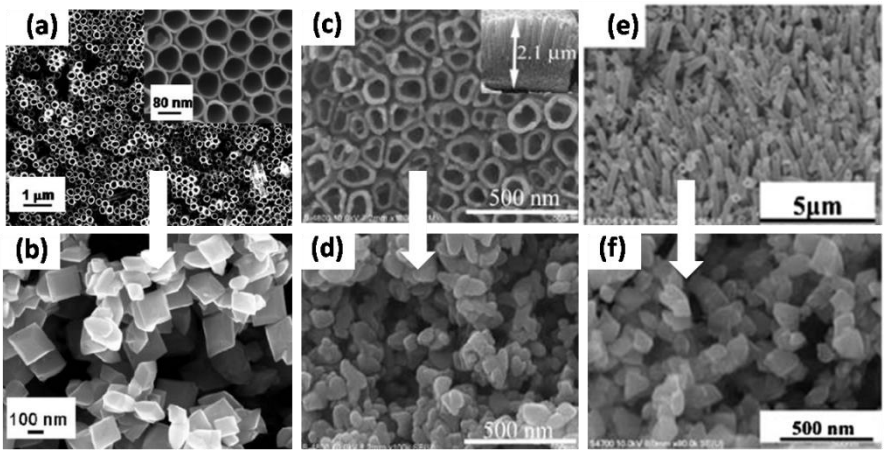

Figure 24. Transformation from as-anodized TiO_2 nanotubes into nanoparticles: (a) and (b) through a thermal annealing of the as-anodized TiO_2 nanotubes in ambient fluorine; (c) and (d) by a 180 C hydrothermal process; (e) and (f) via a treatment in NH_4OH solution prior to calcination. (Reprinted with permission from Reference [277] (a) and (b): Alivov, Y.; Fan, Z. Y. J. Phys. Chem. C 2009, 113, 12954-12957. Reference [278] (c) and (d):Yu, J. G. et al., J. Phys. Chem. C 2010, 114, 19378-19385. Reference [280] (e) and (f): Shokuhfar, T. et al. J. Appl. Phys. 2010, 108. Copyright © American Chemical Society and American Institute of Physics).

nanoparticle [290-292], nanofiber/ nanoparticle [293], nanotube/ nanorod [294], nanorod/ nanofiber [295], and nanobelt/ nanoparticle pairs [28]. For example, a common combination of TiO_2 nanotubes and nanoparticles was realized by treating the as-anodized nanotubes with $TiCl_4$ solution hydrolysis (see Figure 25), which could increase the nanotube surface area and modify the cracks remaining from annealing, effectively improving the conversion efficiency of the nanotube-based DSSCs [91,296]. In addition, anatase nanoparticles mixed with brookite nanorods were obtained by thermal hydrolysis of aqueous solutions of titanium bis (ammonium lactate) dihydroxide in the presence of an optimized concentration of urea, and they exhibited a higher photocatalytic hydrogen evolution activity than that of pure anatase nanoparticles despite the lower surface area of the former. This behavior can be due to the fact that the flatband potential of the brookite nanorods was shifted by 140 mV more cathodically than the flatband potential of the anatase nanoparticles, resulting in higher photocatalytic activity [21]. Moreover, nanoparticle/nanowire composites can possess the advantages of both building blocks, namely, the high surface area of nanoparticle aggregates and the rapid electron transport rate and the light scattering effect of single-crystalline nanowires. Therefore, DSSCs made with these hybrid structures exhibited an enhancement of power

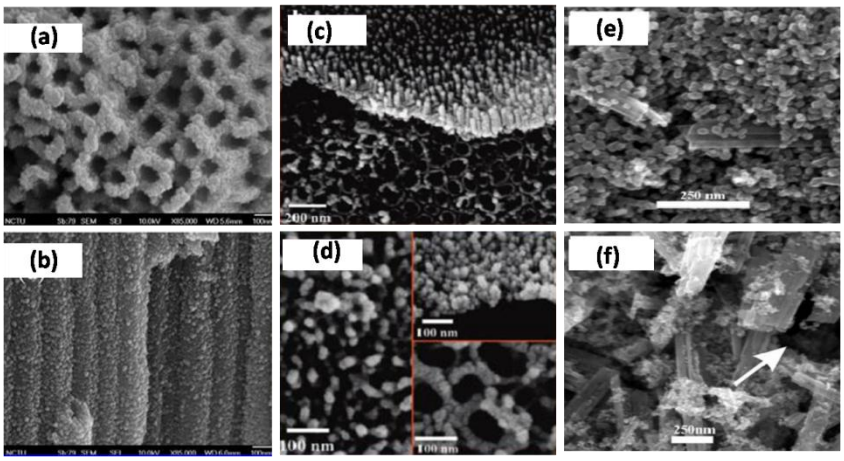

Figure 25. Composition of TiO_2 (a) and (b) nanotubes/nanoparticles; (c) and (d) nanotubes/nanorods; (e) and (f) nanorods/nanoparticles. (Reprinted with permission from Reference [91] (a) and (b): Chen, C. C. et al., J. Phys. Chem. C 2008, 112, 19151-19157. Reference [294] (c) and (d): Zhang, H. M. et al., Langmuir 2010, 26, 11226-11232. Reference [291] (e) and (f): Tan, B.; Wu, Y. Y. J. Phys. Chem. B 2006, 110, 15932-15938. Copyright © American Chemical Society)

efficiency from 6.7% for pure nanoparticle cells to 8.6% for the composite cell with 20 wt % nanowires under 1 Sun AM1.5 illumination (100 mW/cm^2) [291]. Additionally, an optimized composite consisting of electrospun TiO_2 nanofibers and conventional TiO_2 nanoparticles noticeably improved light harvesting due to an increase in scattering without substantially sacrificing the adsorption of dye molecules for the DSSCs, meanwhile, the incorporation of electrospun TiO_2 nanofibers into conventional TiO_2 nanoparticles improved the electron diffusion and transport. Thus, under the same fabrication conditions and film thickness, the DSSC prepared using the composite formed of 15wt% nanofibers and 85wt% nanoparticles demonstrated 44% higher device efficiency (8.8%) than that made using TiO_2 nanoparticles alone (6.1%) [293]. Recently, a novel architecture made of a perpendicularly aligned and highly ordered TiO_2 nanorod/nanotube (NR/NT) adjacent film was obtained by directly anodizing a hydrothermally modified titanium foil with an anatase layer (see Figure 25). The resultant architecture consisted of a highly ordered nanorod top layer that directly joined to a highly ordered nanotube array bottom layer, and the photocatalytic performance toward water and organic compounds demonstrated that photocatalytic oxidation of water of the NT photoanode was almost 1.5 times greater than the NR/NT photoanode. However, the photoactivity of the NR/NT photoanode toward glucose oxidation was nearly 1.4 times higher than that of the NT photoanode. In other words, the NR/NT photoanode possesses the characteristic of selective photocatalytic oxidation toward organics (i.e., glucose), which is beneficial for applications in environmental remediation and analytical determination of organic pollutants, where selective oxidation of organics is highly desirable [294].

5.9. TiO_2 hierarchical structures

Recently, hierarchically structured materials with various morphologies have attracted great attention. The concept of hierarchically organized materials, especially multilevel 3-D organization based on a host macrostructure, allows the 3-D organization necessary for fast mass transport. On this host macrostructure, a secondary guest micro- and/or nanoscale substructure is built in order to take advantage of the properties of nanometer-sized building blocks and micron- or submicron-sized assemblies. The formation of hierarchical structures is generally considered to be a self-assembly process, in which building blocks, such as nanoparticles (0D), nanorods or nanotubes (1D), and nanosheets (2D) self-assemble into regular higher level structures [162,297]. Much effort has been devoted to assembling TiO_2 building blocks into 3-D ordered superstructures or complex functional architectures. For instance, special architectures based on TiO_2 nanorods, such as nanotrees [298], microflowers [299-304], or microspheres [305], and branched nanostructures based on TiO_2 nanowires [306], chestnut-like morphologies with TiO_2 nanopins [307], hierarchical hollow microspheres or branched morphologies [308], assembled by TiO_2 nanotubes, microspheres organized from TiO_2 nanoparticles, TiO_2 nanosheets built from microflowers [309,310], microspherulites [311,312], and mesoporous anatase layers coupled to a three-dimensional photonic crystal architecture [313], have been successfully prepared. To date, many methods for the fabrication of hierarchical geometries are applied and performance improvements have been achieved for solar cell application, despite the fact that the exact assembly mechanisms remain elusive.

Recently, a novel forest-like architecture consisting of hierarchical assemblies of nanocrystalline particles of anatase TiO_2, morphologically resembling a tree, were grown on FTO substrates via pulsed laser deposition (PLD) at room temperature by ablation of a Ti target in a background O_2 atmosphere (see Figure 26). The resulting architecture was proposed to be effective at hampering electron recombination and controlling mass transport in the mesopores, and, thus, achieved a 4.9% conversion efficiency in a DSSC [298]. Moreover, ordered tree-like rutile TiO_2 nanoarrays were developed through a simple, one-pot synthesis approach involving the reaction of a titanium surface with the vapor generated from a hydrochloric acid solution in a hydrothermal process. In addition to tree-like structures, seaweed-like TiO_2 nanoarrays were grown on the surface of a titanium sheet by hydrogen peroxide sculpting at low temperature and exhibited an efficiency of 3.2% for the corresponding DSSC with low recombination rates and long electron life times (see Figure 26) [314]. A chestnut-like morphology with rutile nanopin TiO_2 was also developed from large single crystals of octahedron-like anatase TiO_2 by adjusting the concentration of sodium dodecyl sulfate in the hydrothermal route using aqueous titanium trichloride solutions as precursors (see Figure 26) [307]. Furthermore, TiO_2 nanostrawberry rutile films were fabricated on a large scale from aqueous solution via a sol-gel method with seeded growth at low temperature without any pressure equipment. The behaviors of reversible switching between superhydrophilicity and superhydrophobicity

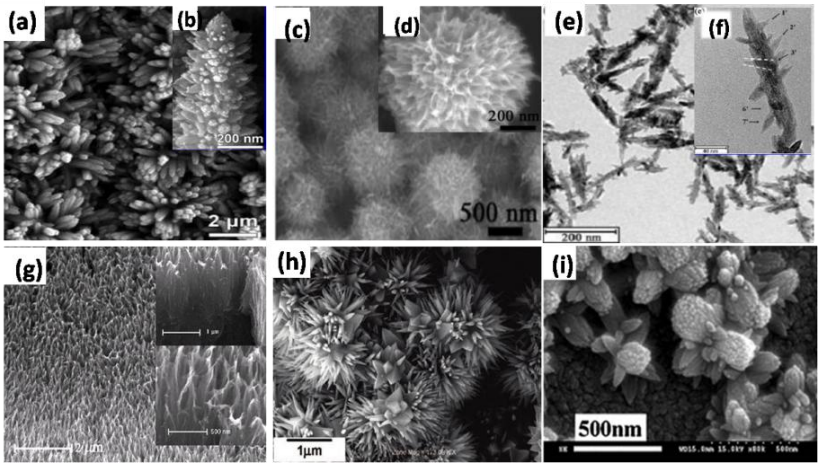

Figure 26. TiO_2 hierarchical structures: (a) and (b) nanotrees; (c) and (d) microspheres; (e) and (f) branched nanorods; (g)seaweed-like; (h) chestnut; (i) nano-strawberry. (Reprinted with permission from Reference [298] (a) and (b): Yang, X. F. et al., Acs Nano 2009, 3, 1212-1218. Reference [305](c) and (d): Wang, C. X. et al., Langmuir 2010, 26, 12841-12848. Reference [306] (e) and (f): Oh, J. K. et al., Chem. Mater. 2010, 22, 1114-1118. Reference [314] (g): Bala, H. et al., Appl. Phys. Lett. 2010, 97. Reference [307](h): Hosono, E. et al., Acs Nano 2007, 1, 273-278. Reference [315] (i): Sun, W. T. et al., Chem. Commun. 2008, 603-605. Copyright © American Chemical Society, American Institute of Physics and Wiley-VCH).

were observed on the film, due to the special structure and native wettability of the TiO_2 (see Figure 26) [315].

6. Summary

Over the past years, the numerous efforts devoted to TiO_2 nanomaterials have enriched knowledge of their synthesis, properties, modification, and applications. Continuing breakthroughs in synthesis technology has introduced new TiO_2 nanostructures, which exhibit the well-known quantum-confinement effect and size/shape-dependent properties as well as unique optical, electronic, thermal, and structural properties, while still possessing high photocatalytic activity. Exploitation of novel architectures including nanorods, nanotubes, and nanowires as well as mesoporous and hierarchical structures will continue, accompanied by progress in manufacturing techniques. Therefore, TiO_2 will likely play an important role in the remediation of environmental pollutants and in the search for renewable and clean energy devices in the near future.

References

1. Fujishima, A., Honda, K., Nature 238 (1972) 37.
2. Wold, A., Chem. Mater. 5 (1993) 280.
3. Liu, G., Wang, L. Z., Yang, H. G., Cheng, H. M., Lu, G. Q. J., Mater. Chem. 20 (2010) 831.
4. Chen, X., Mao, S. S., Chem. Rev. 107 (2007) 2891.
5. Zhang, H. J., Chen, G. H., Bahnemann, D. W., J. Mater. Chem. 19 (2009) 5089.
6. Halme, J., Vahermaa, P., Miettunen, K., Lund, P., Adv. Mater. 22 (2010) E210.
7. Nozik, A. J., Nano Lett. 10 (2010) 2735.
8. Rajeshwar, K., de Tacconi, N. R., Chenthamarakshan, C. R., Chem. Mater. 13 (2001) 2765.
9. Li, Y. M., Somorjai, G. A., Nano Lett. 10 (2010) 2289.
10. Kamat, P. V., J. Phys. Chem. C 111 (2007) 2834.
11. Liu, J., Cao, G. Z., Yang, Z. G., Wang, D. H., Dubois, D., Zhou, X. D., Graff, G. L., Pederson, L. R., Zhang, J. G., ChemSusChem 1 (2008) 676.
12. Serrano, E., Rus, G., Garcia-Martinez, J., Renew. Sustain. Energy Rev. 13 (2009) 2373.
13. Levy, B., J. Electroceram. 1 (1997) 239.
14. Gratzel, M., Nature 414 (2001) 338.
15. Chen, X. B., Chin. J. Catal. 30 (2009) 839.
16. Chen, S. S., Zhu, Y. H., Li, W., Liu, W. J., Li, L. C., Yang, Z. H., Liu, C., Yao, W. J., Lu, X. H., Feng, X., Chin. J. Catal. 31 (2010) 605.
17. Akpan, U. G., Hameed, B. H., J. Hazard. Mater. 170 (2009) 520.
18. Zhang, H. Z., Banfield, J. F., J. Phys. Chem. B 104 (2000) 3481.
19. Finnegan, M. P., Zhang, H. Z., Banfield, J. F., J. Phys. Chem. C 111 (2007) 1962.
20. Zhang, H. Z., Banfield, J. F., J. Mater. Chem. 8 (1998) 2073.

21. Kandiel, T. A., Feldhoff, A., Robben, L., Dillert, R., Bahnemann, D. W., Chem. Mater. 22 (2010) 2050.
22. Ranade, M. R., Navrotsky, A., Zhang, H. Z., Banfield, J. F., Elder, S. H., Zaban, A., Borse, P. H., Kulkarni, S. K., Doran, G. S., Whitfield, H. J., PNAS 99 (2002) 6476.
23. Zhang, H. Z., Banfield, J. F., J. Mater. Res. 15 (2000) 437.
24. Nah, Y. C., Paramasivam, I., Schmuki, P., ChemPhysChem 11 (2010) 2698.
25. Naicker, P. K., Cummings, P. T., Zhang, H. Z., Banfield, J. F., J. Phys. Chem. B 109 (2005) 15243.
26. Park, N. G., van de Lagemaat, J., Frank, A. J., J. Phys. Chem. B 104 (2000) 8989.
27. Wu, J. M., Shih, H. C., Tseng, Y. K., Hsu, C. L., Tsay, C. Y., J. Electrochem. Soc. 154 (2007) H157.
28. Pan, K., Dong, Y. Z., Tian, C. G., Zhou, W., Tian, G. H., Zhao, B. F., Fu, H. G., Electrochim. Acta 54 (2009) 7350.
29. Hu, W. B., Li, L. P., Li, G. S., Tang, C. L., Sun, L., Cryst. Growth Des. 9 (2009) 3676.
30. Liu, Z. Y., Zhang, X. T., Nishimoto, S., Jin, M., Tryk, D. A., Murakami, T., Fujishima, A., Langmuir 23 (2007) 10916.
31. Quinonez, C., Vallejo, W., Gordillo, G., Appl. Surf. Sci. 256 (2010) 4065.
32. Zhang, H. Z., Banfield, J. F., Chem. Mater. 14 (2002) 4145.
33. Ke, T. Y., Peng, C. W., Lee, C. Y., Chiu, H. T., Sheu, H. S., Crystengcomm 11 (2009) 1691.
34. Hsiao, P. T., Tung, Y. L., Teng, H. S., J. Phys. Chem. C 114 (2010) 6762.
35. Tsakalakos, L., Mater. Sci. Eng. R 62 (2008) 175.
36. Paronyan, T. M., Kechiantz, A. M., Lin, M. C., Nanotechnology 19 (2008) 115201.
37. He, X. S., Hu, C. G., Feng, B., Wan, B. Y., Tian, Y. S., J. Electrochem. Soc. 157 (2010) J381.
38. Han, Y. G., Wu, G., Wang, M., Chen, H. Z., Nanotechnology 20 (2009) 235605.
39. Toivola, M., Halme, J., Miettunen, K., Aitola, K., Lund, P. D., Int. J. Energy Res. 33 (2009) 1145.
40. Oregan, B., Gratzel, M., Nature 353 (1991) 737.
41. Snaith, H. J., Schmidt-Mende, L., Adv. Mater. 19 (2007) 3187.
42. Hagfeldt, A., Boschloo, G., Sun, L. C., Kloo, L., Pettersson, H., Chem. Rev. 110 (2010) 6595.
43. Yum, J. H., Chen, P., Gratzel, M., Nazeeruddin, M. K., ChemSusChem 1 (2008) 699.
44. Peter, L., Accounts Chem. Res. 42 (2009) 1839.
45. Spitler, M. T., Parkinson, B. A., Accounts Chem. Res. 42 (2009) 2017.
46. Yanagida, S., Yu, Y. H., Manseki, K., Accounts Chem. Res. 42 (2009) 1827.
47. Hagfeldt, A., Gratzel, M., Accounts Chem. Res. 33 (2000) 269.
48. Thavasi, V., Renugopalakrishnan, V., Jose, R., Ramakrishna, S., Mater. Sci. Eng. R 63 (2009) 81.
49. Imahori, H., Umeyama, T., Ito, S., Accounts Chem. Res. 242 (2009) 1809.
50. Salant, A., Shalom, M., Hod, I., Faust, A., Zaban, A., Banin, U., Acs Nano 4 (2010) 5962.
51. Mora-Sero, I., Gimenez, S., Fabregat-Santiago, F., Gomez, R., Shen, Q., Toyoda, T., Bisquert, J., Acc. Chem. Res. 42 (2009) 1848.
52. Gonzalez-Pedro, V., Xu, X. Q., Mora-Sero, I., Bisquert, J., Acs Nano 4 (2010) 5783.
53. Boschloo, G., Hagfeldt, A., Accounts Chem. Res. 42 (2009) 1819.
54. O'Regan, B. C., Durrant, J. R., Accounts Chem. Res. 42 (2009) 1799.
55. Kawano, R., Katakabe, T., Shimosawa, H., Nazeeruddin, M. K., Graetzel, M., Matsui, H., Kitamura, T., Tanabe, N., Watanabe, M., Phys. Chem. Chem. Phys. 12 (2010) 1916.
56. Wang, P., Zakeeruddin, S. M., Moser, J. E., Gratzel, M., J. Phys. Chem. B 107 (2003) 13280.
57. Ramasamy, E., Chun, J., Lee, J., Carbon 48 (2010) 4563.
58. Hong, W. J., Xu, +Y. X., Lu, G. W., Li, C., Shi, G. Q., Electrochem. Commun. 10 (2008) 1555.
59. Bisquert, J., Cahen, D., Hodes, G., Ruhle, S., Zaban, A., J. Phys. Chem. B 108 (2004) 8106.
60. Kamat, P. V., Tvrdy, K., Baker, D. R., Radich, J. G., Chem. Rev. 110 (2010) 6664.
61. Gratzel, M., Prog. Photovolt.: Res. Appl. 14 (2006) 429.
62. Yerga, R. M. N., Galvan, M. C. A., del Valle, F., de la Mano, J. A. V., Fierro, J. L. G., ChemSusChem 2 (2009) 471.
63. Hu, X. L., Li, G. S., Yu, J. C., Langmuir 26 (2010) 3031.
64. Lee, J. S., Catal. Surv. Asia 9 (2005) 217.
65. Youngblood, W. J., Lee, S. H. A., Maeda, K., Mallouk, T. E., Accounts Chem. Res. 42 (2009) 1966.
66. Chen, X. B., Shen, S. H., Guo, L. J., Mao, S. S., Chem. Rev. 110 (2010) 6503.
67. Galinska, A., Walendziewski, J., Energy Fuels 19 (2005) 1143.
68. Chen, C. C., Ma, W. H., Zhao, J. C., Chem. Soc. Rev. 39 (2010) 4206.
69. Kaur, A., Gupta, U., J. Mater. Chem. 19 (2009) 8279.

70. Shan, A. Y., Ghazi, T. I. M., Rashid, S. A., Appl. Catal. A-Gen. 389 (2010) 1.
71. Shankar, K., Basham, J. I., Allam, N. K., Varghese, O. K., Mor, G. K., Feng, X. J., Paulose, M., Seabold, J. A., Choi, K. S., Grimes, C. A., J. Phys. Chem. C 113 (2009) 6327.
72. Tachikawa, T., Majima, T., Chem. Soc. Rev. 39 (2010) 4802.
73. Tachikawa, T., Fujitsuka, M., Majima, T., J. Phys. Chem. C 111 (2007) 5259.
74. Ismagilov, Z. R., Tsikoza, L. T., Shikina, N. V., Zarytova, V. F., Zinoviev, V. V., Zagrebelnyi, S. N., Russ. Chem. Rev. 78 (2009) 873.
75. Lee, S., Cho, I. S., Lee, J. H., Kim, D. H., Kim, D. W., Kim, J. Y., Shin, H., Lee, J. K., Jung, H. S., Park, N. G., Kim, K., Ko, M. J., Hong, K. S., Chem. Mater. 22 (2010) 1958.
76. Dai, S. X., Wu, Y. Q., Sakai, T., Du, Z. L., Sakai, H., Abe, M., Nanoscale Res. Lett. 5 (2010) 1829.
77. Wu, J. M., Zhang, T. W., Zeng, Y. W., Hayakawa, S., Tsuru, K., Osaka, A., Langmuir 21 (2005) 6995.
78. Gong, D., Grimes, C. A., Varghese, O. K., Hu, W. C., Singh, R. S., Chen, Z., Dickey, E. C., J. Mater. Res. 16 (2001) 3331.
79. Mor, G. K., Varghese, O. K., Paulose, M., Shankar, K., Grimes, C. A., Sol. Energy Mater. Sol. Cells 90 (2006) 2011.
80. Yang, L. X., Luo, S. L., Cai, Q. Y., Yao, S. Z., Chin. Sci. Bull. 55 (2010) 331.
81. Rani, S., Roy, S. C., Paulose, M., Varghese, O. K., Mor, G. K., Kim, S., Yoriya, S., LaTempa, T. J., Grimes, C. A., Phys. Chem. Chem. Phys. 12 (2010) 2780.
82. Albu, S. P., Roy, P., Virtanen, S., Schmuki, P., Isr. J. Chem. 50 (2010) 453.
83. Shan, A. Y., Ghazi, T. I. M., Rashid, S. A., Appl Catal A-Gen 389 (2010) 1.
84. Seifried, S., Winterer, M., Hahn, H., Chem. Vapor Depos. 6 (2000) 239.
85. Pradhan, S. K., Reucroft, P. J., J. Cryst. Growth 250 (2003) 588.
86. Xiang, B., Zhang, Y., Wang, Z., Luo, X. H., Zhu, Y. W., Zhang, H. Z., Yu, D. P., J. Phys. D-Appl. Phys. 38 (2005) 1152.
87. Ren, X., Gershon, T., Iza, D. C., Munoz-Rojas, D., Musselman, K., MacManus-Driscoll, J. L., Nanotechnology 20 (2009) 365604.
88. Yodyingyong, S., Zhou, X. Y., Zhang, Q. F., Triampo, D., Xi, J. T., Park, K., Limketkai, B., Cao, G. Z., J. Phys. Chem. C 114 (2010) 21851.
89. Isley, S. L., Penn, R. L., J. Phys. Chem. B 110 (2006) 15134.
90. Isley, S. L., Penn, R. L., J. Phys. Chem. C 112 (2008) 4469.
91. Chen, C. C., Chung, H. W., Chen, C. H., Lu, H. P., Lan, C. M., Chen, S. F., Luo, L., Hung, C. S., Diau, E. W. G., J. Phys. Chem. C 112 (2008) 19151.
92. Zhang, H. Z., Chen, B., Banfield, J. F., Phys. Chem. Chem. Phys. 11 (2009) 2553.
93. Chen, B., Zhang, H., Dunphy-Guzman, K. A., Spagnoli, D., Kruger, M. B., Muthu, D. V. S., Kunz, M., Fakra, S., Hu, J. Z., Guo, Q. Z., Banfield, J. F., Phys. Rev. B 79 (2009) 125406.
94. Kumar, C. P., Gopal, N. O., Wang, T. C., Wong, M. S., Ke, S. C., J. Phys. Chem. B 110 (2006) 5223.
95. Lana-Villarreal, T., Mao, Y. B., Wong, S. S., Gomez, R., Nanoscale 2 (2010) 1690.
96. Du, L. C., Weng, Y. X., J. Phys. Chem. C 111 (2007) 4567.
97. French, R. A., Jacobson, A. R., Kim, B., Isley, S. L., Penn, R. L., Baveye, P. C., Environ. Sci. Technol. 43 (2009) 1354.
98. Oskam, G., Nellore, A., Penn, R. L., Searson, P. C., J. Phys. Chem. B 107 (2003) 1734.
99. Gutierrez, J., Tercjak, A., Mondragon, I., J. Am. Chem. Soc. 132 (2010) 873.
100. Zhang, H. Z., Finnegan, M., Banfield, J. F., Nano Lett. 1 (2001) 81.
101. Yen, W. C., Lee, Y. H., Lin, J. F., Dai, C. A., Jeng, U. S., Su, W. F., Langmuir 27 (2011) 109.
102. Isley, S. L., Jordan, D. S., Penn, R. L., Mater. Res. Bull. 44 (2009) 119.
103. Penn, R. L., Banfield, J. F., Geochim. Cosmochim. Acta 63 (1999) 1549.
104. Oh, J. K., Lee, J. K., Kim, S. J., Park, K. W., J. Ind. Eng. Chem. 15 (2009) 270.
105. Liu, J. J., Qin, W., Zuo, S. L., Yu, Y. C., Hao, Z. P., J. Hazard. Mater. 163 (2009) 273.
106. Murakami, N., Kurihara, Y., Tsubota, T., Ohno, T., J. Phys. Chem. C 113 (2009) 3062.
107. Yuwono, A. H., Zhang, Y., Wang, J., Zhang, X. H., Fan, H. M., Ji, W., Chem. Mater. 18 (2006) 5876.
108. Cheng, H. M., Ma, J. M., Zhao, Z. G., Qi, L. M., Chem. Mater. 7 (1995) 663.
109. Testino, A., Bellobono, I. R., Buscaglia, V., Canevali, C., D'Arienzo, M., Polizzi, S., Scotti, R., Morazzoni, F., J. Am. Chem. Soc. 129 (2007) 3564.
110. Finnegan, M. P., Zhang, H. Z., Banfield, J. F., Chem. Mater. 20 (2008) 3443.
111. Reyes-Coronado, D., Rodriguez-Gattorno, G., Espinosa-Pesqueira, M. E., Cab, C., de Coss, R., Oskam, G., Nanotechnology 19 (2008) 145605.

112. Luo, M., Cheng, K., Weng, W. J., Song, C. L., Du, P. Y., Shen, G., Xu, G., Han, G. R., Nanotechnology 20 (2009) 215605.
113. Gamez, F., Plaza-Reyes, A., Hurtado, P., Guillen, F., Anta, J. A., Martinez-Haya, B., Perez, S., Sanz, M., Castillejo, M., Izquierdo, J. G., Banares, L., J. Phys. Chem. C 114 (2010) 17409.
114. Sanz, M., Walczak, M., de Nalda, R., Oujja, M., Marco, J. F., Rodriguez, J., Izquierdo, J. G., Banares, L., Castillejo, M., Appl. Surf. Sci. 255 (2009) 5206.
115. Sanz, M., Walczak, M., Oujja, M., Cuesta, A., Castillejo, M., Thin Solid Films 517 (2009) 6546.
116. Barbe, C. J., Arendse, F., Comte, P., Jirousek, M., Lenzmann, F., Shklover, V., Gratzel, M., J. Am. Ceram. Soc. 80 (1997) 3157.
117. Chou, T. P., Zhang, Q. F., Russo, B., Fryxell, G. E., Cao, G. Z., J. Phys. Chem. C 111 (2007) 6296.
118. Gratzel, M., J. Photochem. Photobiol. C-Photochem. Rev. 4 (2003) 145.
119. Gregg, B. A., Coord. Chem. Rev. 248 (2004) 1215.
120. Du, L. C., Furube, A., Hara, K., Katoh, R., Tachiya, M., J. Phys. Chem. C 114 (2010) 8135.
121. Bleta, R., Alphonse, P., Lorenzato, L., J. Phys. Chem. C 114 (2010) 2039.
122. Mukherjee, B., Karthik, C., Ravishankar, N., J. Phys. Chem. C 113 (2009) 18204.
123. Bell, T. D. M., Pagba, C., Myahkostupov, M., Hofkens, J., Piotrowiak, P., J. Phys. Chem. B 110 (2006) 25314.
124. Agarwala, S., Kevin, M., Wong, A. S. W., Peh, C. K. N., Thavasi, V., Ho, G. W., ACS Appl. Mater. Interfaces 2 (2010) 1844.
125. Zukalova, M., Zukal, A., Kavan, L., Nazeeruddin, M. K., Liska, P., Gratzel, M., Nano Lett. 5 (2005) 1789.
126. Hartmann, P., Lee, D. K., Smarsly, B. M., Janek, J., Acs Nano 4 (2010) 3147.
127. Wang, D. H., Ma, Z., Dai, S., Liu, J., Nie, Z. M., Engelhard, M. H., Huo, Q. S., Wang, C. M., Kou, R., J. Phys. Chem. C 112 (2008) 13499.
128. Shao, W., Gu, F., Li, C. Z., Lu, M. K., Ind. Eng. Chem. Res. 49 (2010) 9111.
129. Zhao, X., Liu, M. H., Zhu, Y. F., Thin Solid Films 515 (2007) 7127.
130. Kim, D., Roy, P., Lee, K., Schmuki, P., Electrochem. Commun. 12 (2010) 574.
131. Yang, W. G., Wan, F. R., Chen, Q. W., Li, J. J., Xu, D. S., J. Mater. Chem. 20 (2010) 2870.
132. Chen, D. H., Huang, F. Z., Cheng, Y. B., Caruso, R. A., Adv. Mater. 21 (2009) 2206.
133. Jung, H. G., Kang, Y. S., Sun, Y. K., Electrochim. Acta 55 (2010) 637.
134. Sauvage, F., Chen, D. H., Comte, P., Huang, F. Z., Heiniger, L. P., Cheng, Y. B., Caruso, R. A., Graetzel, M., Acs Nano 4 (2010) 420.
135. Kim, Y. J., Lee, M. H., Kim, H. J., Lim, G., Choi, Y. S., Park, N. G., Kim, K., Lee, W. I., Adv. Mater. 21 (2009) 3668.
136. Zhang, Y. C., Shi, Y. F., Liou, Y. H., Sawvel, A. M., Sun, X. H., Cai, Y., Holden, P. A., Stucky, G. D., J. Mater. Chem. 20 (2010) 4162.
137. Chen, D. H., Cao, L., Huang, F. Z., Imperia, P., Cheng, Y. B., Caruso, R. A., J. Am. Chem. Soc. 132 (2010) 4438.
138. Lu, X. J., Huang, F. Q., Mou, X. L., Wang, Y. M., Xu, F. F., Adv. Mater. 22 (2010) 3719.
139. Kim, Y. J., Chai, S. Y., Lee, W. I., Langmuir 23 (2007) 9567.
140. Yu, J. G., Guo, H. T., Davis, S. A., Mann, S., Adv. Funct. Mater. 16 (2006) 2035.
141. Yang, S. C., Yang, D. J., Kim, J., Hong, J. M., Kim, H. G., Kim, I. D., Lee, H., Adv. Mater. 20 (2008) 1059.
142. Feng, X. A., Yang, L., Liu, Y. L., Appl. Surf. Sci. 257 (2010) 756.
143. Mao, Y. B., Kanungo, M., Hemraj-Benny, T., Wong, S. S., J. Phys. Chem. B 110 (2006) 702.
144. Luo, J. Q., Gao, L., J. Alloy. Compd 487 (2009) 763.
145. Zhang, H. M., Han, Y. H., Liu, X. L., Liu, P. R., Yu, H., Zhang, S. Q., Yao, X. D., Zhao, H. J., Chem. Commun. (2010) 8395.
146. Liu, L., Zhao, Y. P., Liu, H. J., Kou, H. Z., Wang, Y. Q., Nanotechnology 17 (2006) 5046.
147. Tan, Y. F., Yang, L., Chen, J. Z., Qiu, Z., Langmuir 26 (2010) 10111.
148. Sang, Y., Geng, B. Y., Yang, J., Nanoscale 2 (2010) 2109.
149. Shibata, T., Sakai, N., Fukuda, K., Ebina, Y., Sasaki, T., Phys. Chem. Chem. Phys. 9 (2007) 2413.
150. Sasaki, T., Watanabe, M., J. Phys. Chem. B 101 (1997) 10159.
151. Yu, J. G., Fan, J. J., Lv, K. L., Nanoscale 2 (2010) 2144.
152. Vittadini, A., Casarin, M., Theor. Chem. Acc. 120 (2008) 551.
153. He, T., Pan, F. C., Xi, Z. X., Zhang, X. J., Zhang, H. Y., Wang, Z. H., Zhao, M. W., Yan, S. S., Xia, Y. Y., J. Phys. Chem. C 114 (2010) 9234.
154. Wen, P. H., Itoh, H., Tang, W. P., Feng, Q., Langmuir 23 (2007) 11782.
155. Wen, P. H., Itoh, H., Feng, Q., Chem. Lett. 35 (2006) 1226.

156. He, T., Zhao, M. W., Zhang, X. J., Zhang, H. Y., Wang, Z. H., Xi, Z. X., Liu, X. D., Yan, S. S., Xia, Y. Y., Mei, L. M., J. Phys. Chem. C 113 (2009) 13610.
157. Hosono, E., Matsuda, H., Honma, I., Ichihara, M., Zhou, H., Langmuir 23 (2007) 7447.
158. Chen, J. S., Lou, X. W., Electrochem. Commun. 11 (2009) 2332.
159. Yang, H. G., Sun, C. H., Qiao, S. Z., Zou, J., Liu, G., Smith, S. C., Cheng, H. M., Lu, G. Q., Nature 453 (2008) 638.
160. Xiang, Q. J., Lv, K. L., Yu, J. G., Appl. Catal. B-Environ. 96 (2010) 557.
161. Tiano, A. L., Koenigsmann, C., Santulli, A. C., Wong, S. S., Chem. Commun. 46 (2010) 8093.
162. Centi, G., Perathoner, S., Eur. J. Inorg. Chem. (2009) 3851.
163. Zhou, W. J., Liu, H., Boughton, R. I., Du, G. J., Lin, J. J., Wang, J. Y., Liu, D., J. Mater. Chem. 20 (2010) 5993.
164. Yu, K. H., Chen, J. H., Nanoscale Res. Lett. 4 (2009) 1.
165. Bavykin, D. V., Friedrich, J. M., Walsh, F. C., Adv. Mater. 18 (2006) 2807.
166. Ferrari, A. M., Lessio, M., Szieberth, D., Maschio, L., J. Phys. Chem. C 114 (2010) 21219.
167. Evarestov, R. A., Zhukovskii, Y. F., Bandura, A. V., Piskunov, S., J. Phys. Chem. C 114 (2010) 21061.
168. Jennings, J. R., Ghicov, A., Peter, L. M., Schmuki, P., Walker, A. B., J. Am. Chem. Soc. 130 (2008) 13364.
169. Allam, N. K., El-Sayed, M. A., J. Phys. Chem. C 114 (2010) 12024.
170. Xia, D. Y., Jiang, Y. B., He, X. A., Brueck, S. R., J. Appl. Phys. Lett. 97 (2010) 223106.
171. Xu, C. K., Shin, P. H., Cao, L. L., Wu, J. M., Gao, D., Chem. Mater. 22 (2010) 143.
172. Rattanavoravipa, T., Sagawa, T., Yoshikawa, S., Sol. Energy Mater. Sol. Cells 92 (2008) 1445.
173. Mor, G. K., Varghese, O. K., Paulose, M., Shankar, K., Grimes, C. A., Sol. Energ. Mat. Sol. C. 90 (2006) 2011.
174. Mor, G. K., Shankar, K., Paulose, M., Varghese, O. K., Grimes, C. A., Nano Lett. 6 (2006) 215.
175. Paulose, M., Shankar, K., Varghese, O. K., Mor, G. K., Grimes, C. A., J. Phys. D-Appl. Phys. 39 (2006) 2498.
176. Zhou, W. J., Liu, H., Boughton, R. I., Du, G. J., Lin, J. J., Wang, J. Y., Liu, D., J. Mater. Chem. 20 (2010) 5993.
177. Nakahira, A., Kubo, T., Numako, C., Inorg. Chem. 49 (2010) 5845.
178. Suzuki, Y., Yoshikawa, S., J. Mater. Res. 19 (2004) 982.
179. Huang, J. Q., Cao, Y. G., Wang, M. L., Huang, C. G., Deng, Z. H., Tong, H., Liu, Z. G., J. Phys. Chem. C 114 (2010) 14748.
180. Bavykin, D. V., Kulak, A. N., Walsh, F. C., Cryst. Growth Des. 10 (2010) 4421.
181. Wang, W. Z., Varghese, O. K., Paulose, M., Grimes, C. A., Wang, Q. L., Dickey, E., C. J., Mater. Res. 19 (2004) 417.
182. Yang, L. X., Luo, S. L., Cai, Q. Y., Yao, S. Z., Chinese Sci. Bull. 55 (2010) 331.
183. Ruan, C. M., Paulose, M., Varghese, O. K., Mor, G. K., Grimes, C. A., J. Phys. Chem. B 109 (2005) 15754.
184. Allam, N. K., Grimes, C. A., J. Phys. Chem. C 111 (2007) 13028.
185. Allam, N. K., Shankar, K., Grimes, C. A., J. Mater. Chem. 18 (2008) 2341.
186. Yoriya, S., Grimes, C. A., J. Mater. Chem. 21 (2011) 102.
187. Chen, J. F., Lin, J., Chen, X. F., J. Nanomater. (2010) 753253.
188. Li, L. L., Tsai, C. Y., Wu, H. P., Chen, C. C., Diau, E. W. G., J. Mater. Chem. 20 (2010) 2753.
189. Zhang, L., Han, Y., Nanotechnology 21 (2010) 055602.
190. Stergiopoulos, T., Valota, A., Likodimos, V., Speliotis, T., Niarchos, D., Skeldon, P., Thompson, G. E., Falaras, P., Nanotechnology 20 (2009) 365601.
191. Liu, Z. Y., Misra, M., Nanotechnology 21 (2010) 125703.
192. Sun, L. D., Zhang, S., Sun, X. W., Wang, X. Y., Cai, Y. L., Langmuir 26 (2010) 18424.
193. Valota, A., LeClere, D. J., Hashimoto, T., Skeldon, P., Thompson, G. E., Berger, S., Kunze, J., Schmuki, P., Nanotechnology 19 (2008) 355701.
194. Wang, J., Lin, Z. Q., J. Phys. Chem. C 113 (2009) 4026.
195. Wang, J., Zhao, L., Lin, V. S. Y., Lin, Z. Q., J. Mater. Chem. 19 (2009) 3682.
196. Albu, S. P., Ghicov, A., Aldabergenova, S., Drechsel, P., LeClere, D., Thompson, G. E., Macak, J. M., Schmuki, P., Adv. Mater. 20 (2008) 4135.
197. Mohammadpour, A., Waghmare, P. R., Mitra, S. K., Shankar, K., Acs Nano 4 (2010) 7421.
198. Yoriya, S., Grimes, C. A., Langmuir 26 (2010) 417.
199. Varghese, O. K., Paulose, M., Grimes, C. A., Nat. Nanotechnol. 4 (2009) 592.
200. Biswas, S., Shahjahan, M., Hossain, M. F., Takahashi, T., Electrochem. Commun. 12 (2010) 668.
201. Chen, C. H., Chen, K. C., He, J. L., Curr. Appl. Phys. 10 (2010) S176.

202. Tang, Y. X., Tao, J., Tao, H. J., Wu, T., Wang, L., Zhang, Y. Y., Li, Z. L., Tian, X. L., Acta Phys.-Chim. Sin. 24 (2008) 1120.
203. Leenheer, A. J., Miedaner, A., Curtis, C. J., van Hest, M., Ginley, D. S., J. Mater. Res. 22 (2007) 681.
204. Mor, G. K., Varghese, O. K., Paulose, M., Grimes, C. A., Adv. Funct. Mater. 15 (2005) 1291.
205. Wang, D. A., Yu, B., Wang, C. W., Zhou, F., Liu, W. M., Adv. Mater. 21 (2009) 1964.
206. Zhang, G., Huang, H., Zhang, Y., Chan, H. L. W., Zhou, L., Electrochem. Commun. 9 (2007) 2854.
207. Kang, S. H., Kim, H. S., Kim, J. Y., Sung, Y. E., Nanotechnology 20 (2009) 355307.
208. Lei, B. X., Liao, J. Y., Zhang, R., Wang, J., Su, C. Y., Kuang, D. B., J. Phys. Chem. C 114 (2010) 152283.
209. Lin, J., Chen, J. F., Chen, X. F., Electrochem. Commun. 12 (2010) 1062.
210. Wang, J., Lin, Z. Q., Chem. Mater. 20 (2008) 1257.
211. Lin, C. J., Yu, W. Y., Chien, S. H., J. Mater. Chem. 20 (2010) 1073.
212. Wang, Y. H., Yang, H. X., Liu, Y., Wang, H., Shen, H., Yan, J., Xu, H. M., Prog. Photovoltaics 18 (2010) 285.
213. Wang, Y. H., Yang, H. X., Lu, L., J. Appl. Phys. 108 (2010) 064510.
214. Liu, Z. Y., Misra, M., Acs Nano 4 (2010) 2196.
215. Zou, D. C., Wang, D., Chu, Z. Z., Lv, Z. B., Fan, X., Coord. Chem. Rev. 254 (2010) 1169.
216. Liu, Y., Wang, H., Li, M., Hong, R. J., Ye, Q. H., Zheng, J. M., Shen, H., Appl. Phys. Lett. 95 (2009) 233505.
217. Liu, Y., Li, M., Wang, H., Zheng, J. M., Xu, H. M., Ye, Q. H., Shen, H., J. Phys. D-Appl. Phys. 43 (2010) 205103.
218. Chun, J. Y., Lee, J. W., Eur. J. Inorg. Chem. 2010 (2010) 4251.
219. Hochbaum, A. I., Yang, P. D., Chem. Rev. 110 (2010) 527.
220. Cao, L. Y., Fan, P. Y., Vasudev, A. P., White, J. S., Yu, Z. F., Cai, W. S., Schuller, J. A., Fan, S. H., Brongersma, M. L., Nano Lett. 10 (2010) 439.
221. Hagedorn, K., Forgacs, C., Collins, S., Maldonado, S., J. Phys. Chem. C 114 (2010) 12010.
222. Yang, P. D., Yan, R. X., Fardy, M., Nano Lett. 10 (2010) 1529.
223. Shankar, K., Basham, J. I., Allam, N. K., Varghese, O. K., Mor, G. K., Feng, X. J., Paulose, M., Seabold, J. A., Choi, K. S., Grimes, C. A., J. Phys. Chem. C 113 (2009) 6327.
224. Iacomino, A., Cantele, G., Trani, F., Ninno, D., J. Phys. Chem. C 114 (2010) 12389.
225. Miyauchi, M., Tokudome, H., Appl. Phys. Lett. 91 (2007) 043111.
226. Bae, E., Ohno, T., Appl. Catal. B-Environ. 91 (2009) 634.
227. Bae, E., Murakami, N., Ohno, T., J. Mol. Catal. A-Chem. 300 (2009) 72.
228. Peng, P., Liu, X. D., Sun, C. S., Ma, J. M., Zheng, W. J., J. Solid State Chem. 182 (2009) 1003.
229. Wang, H., Liu, Y., Li, M., Huang, H., Zhong, M. Y., Shen, H., Appl. Phys. A-Mater. Sci. Process. 97 (2009) 25.
230. Ding, K. L., Miao, Z. J., Hu, B. J., An, G. M., Sun, Z. Y., Han, B. X., Liu, Z. M., Langmuir 26 (2010) 10294.
231. Wu, J. M., Qi, B., J. Am. Ceram. Soc. 90 (2007) 657.
232. Wu, J. M., Qi, B., J. Am. Ceram. Soc. 91 (2008) 3961.
233. Koo, B., Park, J., Kim, Y., Choi, S. H., Sung, Y. E., Hyeon, T., J. Phys. Chem. B 110 (2006) 24318.
234. Sedach, P. A., Gordon, T. J., Sayed, S. Y., Furstenhaupt, T., Sui, R. H., Baumgartner, T., Berlinguette, C. P., J. Mater. Chem. 20 (2010) 5063.
235. Das, J., Freitas, F. S., Evans, I. R., Nogueira, A. F., Khushalani, D., J. Mater. Chem. 20 (2010) 4425.
236. Meng, L. J., Ren, T., Li, C., Appl. Surf. Sci. 256 (2010) 3676.
237. Li, Y., Fang, X. S., Koshizaki, N., Sasaki, T., Li, L., Gao, S. Y., Shimizu, Y., Bando, Y., Golberg, D., Adv. Funct. Mater. 19 (2009) 2467.
238. Krause, K. M., Vick, D. W., Malac, M., Brett, M. J., Langmuir 26 (2010) 17558.
239. Kang, S. H., Choi, S. H., Kang, M. S., Kim, J. Y., Kim, H. S., Hyeon, T., Sung, Y. E., Adv. Mater. 20 (2008) 54.
240. Wolcott, A., Smith, W. A., Kuykendall, T. R., Zhao, Y. P., Zhang, J. Z., Small 5 (2009) 104.
241. De Marco, L., Manca, M., Giannuzzi, R., Malara, F., Melcarne, G., Ciccarella, G., Zama, I., Cingolani, R., Gigli, G., J. Phys. Chem. C 114 (2010) 4228.
242. Wu, W. Y., Chang, Y. M., Ting, J. M., Cryst. Growth Des. 10 (2010) 1646.
243. Kumar, A., Madaria, A. R., Zhou, C. W., J. Phys. Chem. C 114 (2010) 7787.
244. Liu, B., Aydil, E. S., J. Am. Chem. Soc. 131 (2009) 3985.
245. Yang, W. G., Wan, F. R., Wang, Y. L., Jiang, C. H., Appl. Phys. Lett. 95 (2009) 133121.

246. Adachi, M., Murata, Y., Takao, J., Jiu, J. T., Sakamoto, M., Wang, F. M., J. Am. Chem. Soc. 126 (2004) 14943.
247. Feng, X. J., Shankar, K., Varghese, O. K., Paulose, M., Latempa, T. J., Grimes, C. A., Nano Lett. 8 (2008) 3781.
248. Zhang, W., Zhu, R., Ke, L., Liu, X. Z., Liu, B., Ramakrishna, S., Small 6 (2010) 2176.
249. Choi, S. K., Kim, S., Lim, S. K., Park, H., J. Phys. Chem. C 114 (2010) 16475.
250. Tetreault, N., Horvath, E., Moehl, T., Brillet, J., Smajda, R., Bungener, S., Cai, N., Wang, P., Zakeeruddin, S. M., Forro, L., Magrez, A., Gratzel, M., Acs Nano 4 (2010) 7644.
251. Yuan, J. J., Jin, R. H., Langmuir 26 (2010) 4212.
252. Reddy, M. V., Jose, R., Teng, T. H., Chowdari, B. V. R., Ramakrishna, S., Electrochim. Acta 55 (2010) 3109.
253. Zhan, S. H., Chen, D. R., Jiao, X. L., Tao, C. H., J. Phys. Chem. B 110 (2006) 11199.
254. Fei, H. H., Yang, Y. C., Rogow, D. L., Fan, X. J., Oliver, S. R. J., ACS Appl. Mater. Interfaces 2 (2010) 974.
255. Qu, Y., Zhou, W., Pan, K., Tian, C. G., Ren, Z. Y., Dong, Y. Z., Fu, H. G., Phys. Chem. Chem. Phys. 12 (2010) 9205.
256. Liu, J. J., Dong, M. Q., Zuo, S. L., Yu, Y. C., Appl. Clay Sci. 43 (2009) 156.
257. Cesano, F., Bertarione, S., Damin, A., Agostini, G., Usseglio, S., Vitillo, J. G., Lamberti, C., Spoto, G., Scarano, D., Zecchina, A., Adv. Mater. 20 (2008) 3342.
258. Chen, Y., Park, S. M., Kim, H. C., McVittie, J. P., Ting, C., Nish, Y., J. Electrochem. Soc. 157 (2010) E155.
259. Qiu, Y. C., Chen, W., Yang, S. H., Angew. Chem.-Int. Edit. 49 (2010) 3675.
260. Li, J. M., Yu, Y. X., Chen, Q. W., Li, J. J., Xu, D. S., Cryst. Growth Des. 10 (2010) 2111.
261. Qiu, Y. C., Yan, K. Y., Yang, S. H., Jin, L. M., Deng, H., Li, W. S., Acs Nano 4 (2010) 6515.
262. Chen, Y., Kim, H. C., McVittie, J., Ting, C., Nishi, Y., Nanotechnology 21 (2010) 185303.
263. Deng, Q. X., Wei, M. D., Ding, X. K., Jiang, L. L., Wei, K. W., Zhou, H. S., J. Cryst. Growth 312 (2010) 213.
264. Nair, A. S., Yang, S. Y., Zhu, P. N., Ramakrishna, S., Chem. Commun. 46 (2010) 7421.
265. Peng, H. R., Wang, X. C., Li, G. C., Pang, H. T., Chen, X. G., Mater. Lett. 64 (2010) 1898.
266. Li, X. L., Peng, Q., Yi, J. X., Wang, X., Li, Y. D., Chem.-Eur. J. 12 (2006) 2383.
267. Peng, X. S., Wang, J. P., Thomas, D. F., Chen, A. C., Nanotechnology 16 (2005) 2389.
268. Song, X. M., Wu, J. M., Yan, M., Thin Solid Films 517 (2009) 4341.
269. Li, J. G., Ishigaki, T., Sun, X. D., J. Phys. Chem. C 111 (2007) 4969.
270. Xu, Y. M., Fang, X. M., Xiong, J. A., Zhang, Z. G., Mater. Res. Bull. 45 (2010) 799.
271. Wei, W., Berger, S., Hauser, C., Meyer, K., Yang, M., Schmuki, P., Electrochem. Commun. 12 (2010) 1184.
272. Peng, X. S., Chen, A. C., Adv. Funct. Mater. 16 (2006) 1355.
273. Shen, L. M., Bao, N. Z., Zheng, Y. Q., Gupta, A., An, T. C., Yanagisawa, K., J. Phys. Chem. C 112 (2008) 8809.
274. Suprabha, T., Roy, H. G., Thomas, J., Kumar, K. P., Mathew, S., Nanoscale Res. Lett. 4 (2009) 144.
275. Liu, L., Qian, J. S., Li, B., Cui, Y. M., Zhou, X. F., Guo, X. F., Ding, W. P., Chem. Commun. 46 (2010) 2402.
276. Nian, J. N., Teng, H. S., J. Phys. Chem. B 110 (2006) 4193.
277. Alivov, Y., Fan, Z. Y., J. Mater. Sci. 45 (2010) 2902.
278. Yu, J. G., Dai, G. P., Cheng, B., J. Phys. Chem. C 114 (2010) 19378.
279. Alivov, Y., Fan, Z. Y., J. Phys. Chem. C 113 (2009) 12954.
280. Shokuhfar, T., Gao, Q., Ashtana, A., Walzack, K., Heiden, P., Friedrich, C., J. Appl. Phys. 108 (2010) 104310.
281. Alivov, Y., Fan, Z. Y., Nanotechnology 20 (2009) 405610.
282. Horvath, E., Kukovecz, A., Konya, Z., Kiricsi, I., Chem. Mater. 19 (2007) 927.
283. Xu, H., Tao, X., Wang, D. T., Zheng, Y. Z., Chen, J. F., Electrochim. Acta 55 (2010) 2280.
284. Das, P. P., Mohapatra, S. K., Misra, M., J. Phys. D-Appl. Phys. 41 (2008) 245103.
285. Lee, K. M., Suryanarayanan, V., Huang, J. H., Thomas, K. R. J., Lin, J. T., Ho, K. C., Electrochim. Acta 54 (2009) 4123.
286. Li, X. D., Zhang, D. W., Chen, S., Wang, Z. A., Sun, Z., Yin, X. J., Huang, S. M., Mater. Chem. Phys. 124 (2010) 179.
287. Durr, M., Schmid, A., Obermaier, M., Rosselli, S., Yasuda, A., Nelles, G., Nat. Mater. 4 (2005) 607.
288. Qu, J., Li, G. R., Gao, X. P., Energy Environ. Sci. 3 (2010) 2003.
289. Saji, V. S., Pyo, M., Thin Solid Films 518 (2010) 6542.
290. Yu, C., Park, J., J. Solid State Chem. 183 (2010) 2268.

291. Tan, B., Wu, Y. Y., J. Phys. Chem. B 110 (2006) 15932.
292. Wu, J. J., Chen, G. R., Lu, C. C., Wu, W. T., Chen, J. S., Nanotechnology 19 (2008) 105702.
293. Joshi, P., Zhang, L. F., Davoux, D., Zhu, Z. T., Galipeau, D., Fong, H., Qiao, Q. Q., Energy Environ. Sci. 3 (2010) 1507.
294. Zhang, H. M., Liu, P. R., Liu, X. L., Zhang, S. Q., Yao, X. D., An, T. C., Amal, R., Zhao, H. J., Langmuir 26 (2010) 11226.
295. Shang, M., Wang, W. Z., Yin, W. Z., Ren, J., Sun, S. M., Zhang, L., Chem.-Eur. J. 16 (2010) 11412.
296. Wang, J., Lin, Z. Q., Chem. Mater. 22 (2010) 579.
297. Wu, X. J., Zhu, F., Mu, C., Liang, Y. Q., Xu, L. F., Chen, Q. W., Chen, R. Z., Xu, D. S., Coord. Chem. Rev. 254 (2010) 1135.
298. Yang, X. F., Zhuang, J. L., Li, X. Y., Chen, D. H., Ouyang, G. F., Mao, Z. Q., Han, Y. X., He, Z. H., Liang, C. L., Wu, M. M., Yu, J. C., Acs Nano 3 (2009) 1212.
299. Masuda, Y., Ohji, T., Kato, K., Cryst. Growth Des. 10 (2010) 913.
300. Phan, T. D. N., Pham, H. D., Cuong, T. V., Kim, E. J., Kim, S., Shin, E. W., J. Cryst. Growth 312 (2009) 79.
301. Hyam, R. S., Bhosale, R. K., Lee, W., Han, S. H., Hannoyer, B., Ogale, S. B., J. Nanosci. Nanotechnol. 10 (2010) 5894.
302. Bal, X. L., Xie, B., Pan, N., Wang, X. P., Wang, H. Q., J. Solid State Chem. 181 (2008) 450.
303. Hosono, E., Fujihara, S., Kakiuchi, K., Imai, H., J. Am. Chem. Soc. 126 (2004) 7790.
304. Wang, H. E., Chen, Z. H., Leung, Y. H., Luan, C. Y., Liu, C. P., Tang, Y. B., Yan, C., Zhang, W. J., Zapien, J. A., Bello, I., Lee, S. T., Appl. Phys. Lett. 96 (2010) 263104.
305. Wang, C. X., Yin, L. W., Zhang, L. Y., Qi, Y. X., Lun, N., Liu, N. N., Langmuir 26 (2010) 12841.
306. Oh, J. K., Lee, J. K., Kim, H. S., Han, S. B., Park, K. W., Chem. Mater. 22 (2010) 1114.
307. Hosono, E., Fujihara, S., Lmai, H., Honma, I., Masaki, I., Zhou, H. S., ACS Nano 1 (2007) 273.
308. Zhang, H. M., Liu, P. R., Wang, H. J., Yu, H., Zhang, S. Q., Zhu, H. Y., Peng, F., Zhao, H. J., Langmuir 26 (2010) 1574.
309. Zhu, J., Wang, S. H., Bian, Z. F., Cai, C. L., Li, H. X., Res. Chem. Intermed. 35 (2009) 767.
310. Jitputti, J., Rattanavoravipa, T., Chuangchote, S., Pavasupree, S., Suzuki, Y., Yoshikawa, S., Catal. Commun. 10 (2009) 378.
311. Tang, Y. X., Gong, D. G., Lai, Y. K., Shen, Y. Q., Zhang, Y. Y., Huang, Y. Z., Tao, J., Lin, C. J., Dong, Z. L., Chen, Z., J. Mater. Chem. 20 (2010) 10169.
312. Pavasupree, S., Ngamsinlapasathian, S., Suzuki, Y., Yoshikawa, S., Mater. Lett. 61 (2007) 2973.
313. Guldin, S., Huttner, S., Kolle, M., Welland, M. E., Muller-Buschbaum, P., Friend, R. H., Steiner, U., Tetreault, N., Nano Lett. 10 (2010) 2303.
314. Bala, H., Jiang, L., Fu, W. Y., Yuan, G. Y., Wang, X. D., Liu, Z. R., Appl. Phys. Lett. 97 (2010) 153108.
315. Sun, W. T., Zhou, S. Y., Chen, P., Peng, L. M., Chem. Commun. 603 (2008) 603.

Cite this article as:

Zhiqun Lin *et al.*: **Nanostructured TiO_2 architectures for environmental and energy applications.** *J. Nanosci. Lett.* 2012, **2**: 1